



Assessing the Contributions of Atmospheric/Meteoric Water and Sea Ice Meltwater and Their Influences on Geochemical Properties in Estuaries of the Canadian Arctic Archipelago

Matthew B. Alkire¹ · Andrew Jacobson² · Robie W. Macdonald³ · Gregory Lehn²

Received: 9 July 2018 / Revised: 1 April 2019 / Accepted: 6 April 2019 / Published online: 20 May 2019
© The Author(s) 2019

Abstract

Salinity and stable oxygen isotope ($\delta^{18}\text{O}$) data collected from eight estuaries distributed throughout the Canadian Arctic Archipelago were used to apportion contributions from local meteoric water (MW) and sea ice meltwater (SIM) sources during July and August of 2015 and 2016. The size of the rivers flowing into the estuaries varied by an order of magnitude (in terms of mean annual discharge); however, the inventories of MW were always greater or equal to SIM inventories, indicating that MW was the dominant freshwater source. Residence times of MW generally ranged between 1 and 8 days, with longer times (> 20 days) computed for estuaries in the Somerset Island and Baffin Island regions. Shorter residence times indicate, but do not confirm, that river waters move through the estuaries and proceed offshore relatively quickly. Despite this swift transport, nonconservative behaviors were observed for barium and dissolved organic carbon (DOC). These behaviors were identified via examination of total alkalinity, barium, and DOC concentrations that remained after accounting for contributions from MW and seawater. Remaining concentrations/anomalies that deviated significantly from a linear correlation with SIM were attributed to nonconservative behaviors (e.g., desorption of barium from river-borne particles, remineralization of DOC) or inaccurate assignments of endmember values in the water type analyses. Thus, these anomalies offer a means to better inform water type analyses in the correct assignment of endmember properties that best represent the environment studied.

Keywords Arctic · Freshwater · Estuaries · Water mass mixing · Circulation · Chemical tracers

Introduction

The freshwater budget of the Arctic Ocean has received considerable attention in the scientific literature, in part due to the potential impact that a large export of this freshwater to the North Atlantic might have on the formation of deep and bottom waters

that drive the meridional overturning circulation (Aagaard and Carmack 1989; Proshutinsky et al. 2002; Jungclauss et al. 2006). There are two primary conduits through which freshwater exits the Arctic: Fram Strait and the Canadian Arctic Archipelago (CAA). The exports of freshwater through these channels are approximately equivalent ($2500\text{--}3000\text{ km}^3\text{ year}^{-1}$) (Serreze et al. 2006; Haine et al. 2015); however, the relative composition/source(s) of the freshwater that is exported varies in response to changes in circulation patterns in the Arctic Ocean (e.g., Taylor et al. 2003; Falck et al. 2005; Jahn et al. 2010; Dodd et al. 2012) as well as the gradient in dynamic height between the Arctic and Baffin Bay (e.g., Kliem and Greenberg 2003). In addition to the impact on convective overturning in the North Atlantic, variations in the composition of the freshwater flux have important implications for biological production (Chierici and Fransson 2009; Yamamoto-Kawai et al. 2006; Torres-Valdes et al. 2013) and ocean acidification (Azetsu-Scott et al. 2010; AMAP 2013) downstream in Baffin Bay and the North Atlantic.

The sources of freshwater contributing to the outflow through the CAA include North American river runoff, Siberian river runoff, Pacific water, sea ice meltwater,

Communicated by Nancy L. Jackson

Electronic supplementary material The online version of this article (<https://doi.org/10.1007/s12237-019-00562-w>) contains supplementary material, which is available to authorized users.

✉ Matthew B. Alkire
alkirem@uw.edu

¹ Applied Physics Laboratory, University of Washington, Seattle, WA, USA

² Department of Earth & Planetary Sciences, Northwestern University, Evanston, IL, USA

³ Department of Fisheries & Oceans, Institute of Ocean Sciences, Sidney, BC, Canada

precipitation (minus evaporation, or P-E), and glacial meltwater. Note that Pacific water is considered a freshwater source because its characteristic salinity range ($31.5 \leq S \leq 33$) is lower than that of Atlantic water ($S \geq 34.8$) that contributes to both the Arctic Ocean and Baffin Bay. The North American river runoff component includes contributions from rivers that discharge directly into the Arctic Ocean (e.g., Mackenzie River) and those that discharge into the straits and channels of the CAA (i.e., local rivers) whereas Siberian runoff originates from transport across the Arctic Ocean. It is becoming increasingly important to separate and quantify the contributions of these different sources of freshwater to the export through the CAA as circulation patterns are rapidly changing and most of the freshwater inflows have increased: glacial melt has accelerated (e.g., Rignot et al. 2010; Gardner et al. 2011; Washam et al. 2018), Siberian river discharge has increased (Peterson et al. 2006), North American river discharge rates have become more variable (Déry et al. 2009), sea ice volume and areal coverage continues to decline (Comiso et al. 2008; Stroeve et al. 2011), and the inflow of Pacific water into the Arctic via Bering Strait has grown (Woodgate et al. 2012).

Despite the importance of distinguishing between these freshwater sources, very few data have been collected from the CAA or its local rivers. Recently, Alkire et al. (2017) determined that the mean annual discharge from CAA rivers is on the order of $200\text{--}300 \text{ km}^3 \text{ year}^{-1}$, approximately equal to that of the Mackenzie River. Furthermore, they discovered that the geochemistry of local CAA rivers is both heterogeneous and significantly different from that of larger North American rivers such as the Mackenzie and Yukon Rivers. This information is relevant as runoff from numerous rivers may be combined in coastal currents and nearshore regions such as the “Riverine Coastal Domain,” a narrow and shallow region following the coastlines of Alaska and northern Canada that aggregates runoff (Carmack et al. 2015), where it contributes to the freshwater export through the CAA and masks the chemical signature of runoff derived from Arctic Ocean sources. In fact, previous studies conducted in the CAA suggest freshwater fluxes tend to be concentrated in boundary currents swiftly flowing along the right-hand sides of the channels (relative to the flow direction) toward Baffin Bay and the North Atlantic (Jones and Coote 1980; Melling 2000; Prinsenberg and Hamilton 2005; Melling et al. 2008). Consequently, if one wants to separate and quantify the various contributions of freshwater to the export flux exiting the Arctic via the CAA, it is important to understand both the variations in the geochemical compositions of local CAA rivers (Alkire et al. 2017) as well as the degree to which these compositions may or may not be altered during transport through adjoining estuaries (this study).

Geochemical tracers have been successfully employed to separate and quantify the contributions of different sources to the freshwater fluxes exiting the Arctic Ocean. Salinity and

the stable oxygen isotope composition of water ($\delta^{18}\text{O}$) are frequently used to separate contributions of sea ice meltwater and meteoric water (a classification that includes river runoff, P-E, and glacial meltwater) (e.g., Dodd et al. 2012; Azetsu-Scott et al. 2012). Additional tracers are necessary to allow further separations. For example, total alkalinity and barium have been used to distinguish contributions from North American versus Siberian river runoff in the Arctic Ocean (Yamamoto-Kawai et al. 2005; Guay et al. 2009), Fram Strait (Taylor et al. 2003), and in the CAA (Yamamoto-Kawai et al. 2010). Dissolved organic carbon (DOC) and, in particular, colored dissolved organic matter (CDOM) have also been used to trace river runoff, particularly from Siberian rivers, through the Arctic Ocean and out via Fram Strait (e.g., Guay et al. 1999; Amon et al. 2003; Guéguen et al. 2007; Granskog et al. 2012; McClelland et al. 2012; Ficht et al. 2013; Pavlov et al. 2015). However, the utility of these tracers depends upon conservative behavior during estuarine mixing. In some circumstances, nonconservative behavior can be accounted for, permitting the application of the tracer to discriminate water types. In other circumstances, nonconservative processes restrict or prohibit the application of these tracers to the quantitative separation of different water sources. For example, the desorption of particulate barium carried by the Mackenzie and Yukon Rivers during estuarine mixing significantly increases the dissolved barium concentrations above those of Siberian Rivers, allowing the discrimination of these two freshwater sources (e.g., Guay and Falkner 1997, 1998). In contrast, the apparent remineralization of DOC in the Mackenzie estuary prevents its utility as a tracer of Mackenzie River runoff in Canada Basin (Guay et al. 1999) whereas a larger fraction of DOC presumably passes through Siberian estuaries, allowing for Siberian rivers to be tracked in the Eurasian Basin of the Arctic Ocean and Fram Strait (e.g., Amon et al. 2003; Amon and Meon 2004).

Here, we present an analysis of physical and geochemical data collected from rivers and estuaries that are widely distributed across both northern and southern routes through which Arctic waters may be transported to Hudson and Baffin Bays (Fig. 1). The contributions of fresh water that have entered the Arctic via an atmospheric pathway (i.e., meteoric water, or MW) versus fresh water derived within the Arctic from melting sea ice (SIM) are separated and quantified and the results combined with additional geochemical variables to determine the degree to which these other tracers behave conservatively during estuarine mixing. Tracers that are relatively conservative during their residence times within the estuaries may prove of further use for determining how individual estuaries within the Archipelago contribute to the general transport of runoff and sea ice melt through the CAA to Baffin Bay and Davis Strait within nearshore, boundary currents.

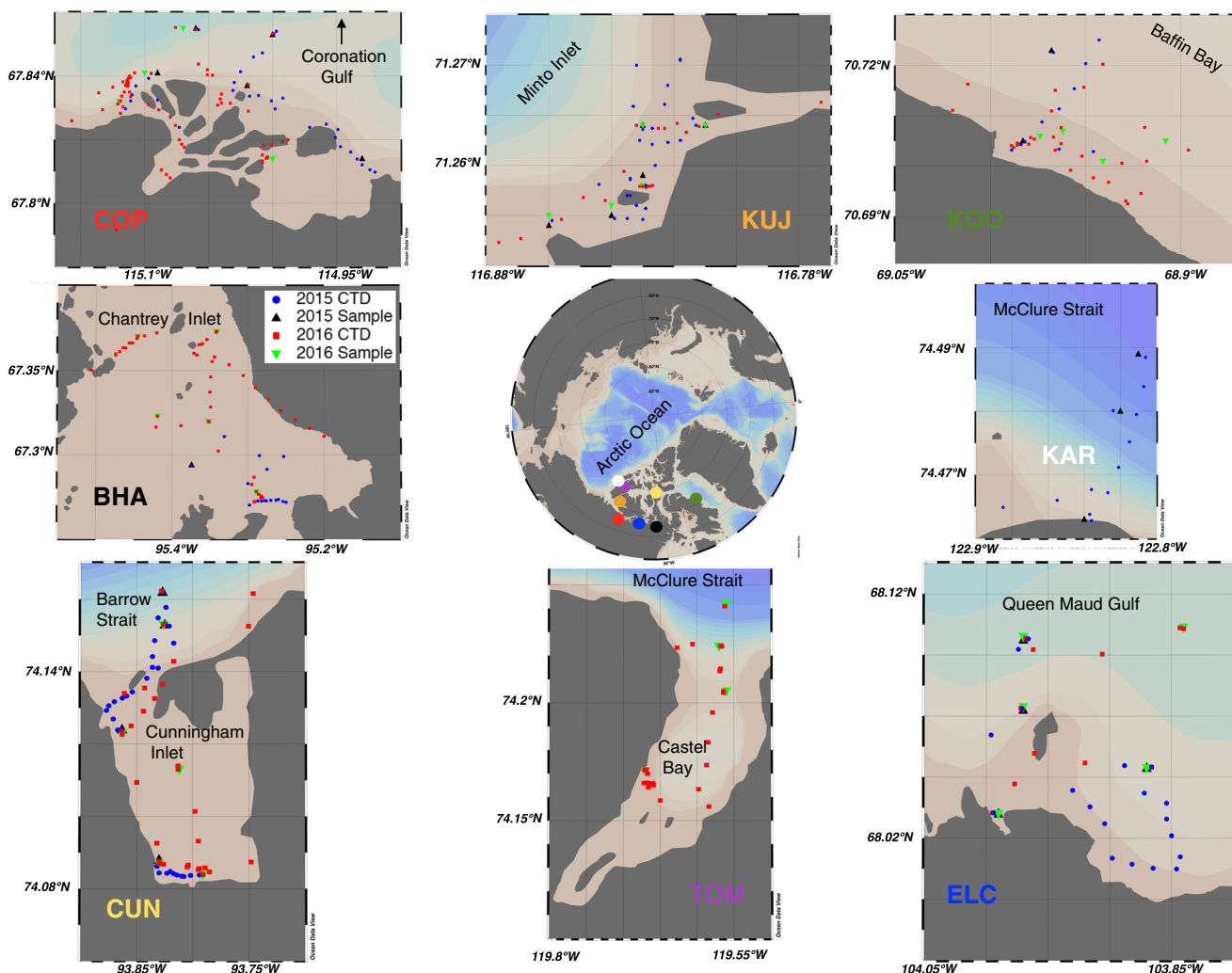


Fig. 1 Maps showing the locations where CTDs were deployed and water samples collected in the various estuaries visited during the study. The central map shows the locations of these estuaries in the Canadian Arctic Archipelago (CAA), with colored dots coded to each estuary. On each estuary map, blue and red symbols indicate locations where CTDs

were used to measure vertical profiles of temperature and salinity in 2015 (blue dots) and 2016 (red squares). Black triangles indicate stations where water samples were collected in 2015 and green, inverted triangles indicate sampling locations in 2016. Maps assembled using Ocean Data View (Schlitzer 2018)

Study Area

Background

Estuaries of the Arctic and subarctic seas receive freshwater inputs from rivers, net precipitation over evaporation, and (in some regions) meltwater input from glacial ice. Collectively, these sources are termed meteoric waters. Sea ice formation and melting also affect the freshwater content of seawater. Specifically, formation of sea ice (freezing of seawater) extracts freshwater from estuaries and oceans during winter, whereas sea ice melt provides a widely distributed source of freshwater during summer. Sea ice therefore complicates the interpretation of freshwater distribution in Arctic estuaries as it cannot be assumed that the freshwater has resulted solely from river runoff. Instead, contributions from sea ice meltwater and

meteoric water (assumed to originate predominately from river runoff in the estuaries) must be distinguished and quantified.

In late winter, shallow Arctic estuaries are characterized by a thick (1–2 m) cover of sea ice, some of which may be frozen directly to the sea bed (termed landfast ice). River discharge is typically very small or entirely absent, as smaller rivers freeze to the bottom during winter months. The water column is expected to be homogeneous in late winter given that winds and atmospheric cooling mix the water column during fall and then, throughout the winter, rivers supply little to support stratification whereas the cumulative release of high-density brines during sea ice formation promotes convection. More saline waters may also be introduced to the estuary from offshore via tides. As the winter gives way to spring, the snow and ice begin to melt.

Rivers typically begin to melt farther upstream (south) and this thawing slowly advances downstream. This progression eventually breaks up the ice near the mouth of the rivers, releasing the volume of water in a turbulent flood. This peak discharge occurs between late May and early June (YDs 160–180) and then declines over the subsequent weeks (Fig. 2). The introduction of freshwater from the spring floods and melting sea ice stratifies the water column into a two-layer, estuarine system with freshwaters typically moving offshore in the surface layer and more saline waters moving onshore in the deeper layer. With the progression into summer, the river discharge declines toward a base flow, supported by summer precipitation, the continuing melt of snow, water stored in lakes, and groundwater. The landfast ice has generally been broken up or melted in place, and freely moving pack ice moves onshore and offshore with tides and prevailing winds. By autumn, river flow has substantially decreased, offering little to no additional freshwater to maintain stratification, and strong winds and cooling temperatures facilitate mixing of the water column. As the temperature continues to decline, sea ice begins to form, distilling the estuary waters such that freshwater is trapped as solid ice and salt is released back to the water column as brines (further contributing to water column homogenization).

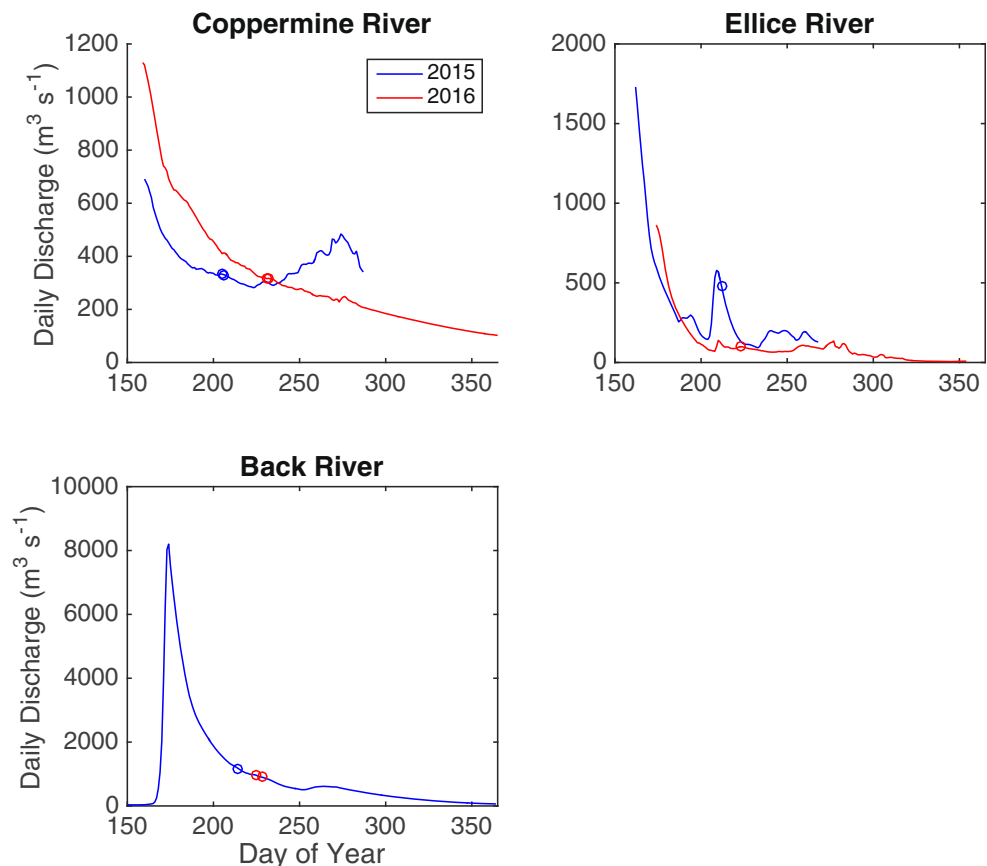
Brief Description of Estuaries

Some of the water bodies surveyed have indigenous names as well as alternative geographical names. For simplicity, we refer to each estuary by the names of the river(s) that discharge into them: Coppermine (COP), Ellice (ELC), Back and Hayes (BHA), Kuujuaa (KUJ), Thomsen (TOM), Cunningham (CUN), Karasok (KAR), and Koogaaluk (KOO).

The Coppermine River flows northward from mainland Nunavut into a small estuary (COP) of Coronation Gulf via multiple channels separated by small islands. The Coppermine River discharge was concentrated in the westernmost channel during both years. This is the deepest channel connecting the Coppermine River to the estuary, and all boat traffic moving between the estuary and river travel within this channel (personal observation). Although river water enters the estuary via the other channels, these are much shallower (this is not obvious from the available bathymetry data). The Coppermine River plume exits via all channels, but the majority of the flow follows the westernmost channel and moves westward along the shore before turning northeastward to flow into the estuary.

The Ellice River flows northward from mainland Nunavut into an estuary (ELC) that is essentially open to Queen Maud Gulf. We encountered the sea ice edge at

Fig. 2 Daily discharge ($\text{m}^3 \text{s}^{-1}$) for the Coppermine, Ellice, and Back Rivers for 2015 (blue) and 2016 (red). Data downloaded from Water Survey of Canada (<https://wateroffice.ec.gc.ca>). Blue and red circles indicate the days water sampling surveys were conducted in the adjoining estuaries during 2015 and 2016, respectively. No data available for the Back River in 2016; however, days of sampling provided for comparison (assuming a similar hydrograph in 2016 as that measured during 2015)



these offshore stations in 2015; however, no sea ice was observed in the region in 2016. The Back and Hayes Rivers flow northward and westward, respectively, from mainland Nunavut into Chantrey Inlet, a relatively protected/isolated estuary (BHA) located south of Boothia Peninsula. Limited sampling was conducted within the estuary in 2015 due to high winds (> 10 knots) that resulted in rough waters within this shallow estuary; therefore, only one full station was occupied, and a surface sample was collected near the mouth of the river.

The Kuujua River flows westward from Victoria Island (Northwest Territories) and empties into Minto Inlet (KUJ) and Amundsen Gulf. The Cunningham River flows northward from Somerset Island (Nunavut) into the Cunningham Inlet (CUN) and Barrow Strait. The estuary/inlet is relatively isolated and only open to the ocean on the northwestern side. This semi-enclosed geometry likely facilitates the retention of sea ice during break up and melt. Since the river discharge is very low, the circulation within the estuary (and residence time of surface waters) is more likely dominated by tidal mixing. A brief analysis of available tidal models as well as the simulation of tidal elevations in nearby Resolute Bay (see Text S3 in the Supplementary Materials) indicates a change in the water level of ~2 m between high and low tide. This relatively large tidal range very likely results in strong tidal currents that move waters into and out of the narrow entrance to the inlet.

The Thomsen River flows northward from Banks Island (Northwest Territories) into Castel Bay (TOM) and McClure Strait. No data were collected from this estuary in 2015 due to unsafe conditions for landing the aircraft; however conditions did allow for the aircraft to land near the estuary in 2016. The Karasok River, located to the west of the Thomsen, also flows northward from Banks Island but empties directly into McClure Strait. Sea ice was prevalent in and around this estuary (KAR) during the 2015 survey. This estuary was not surveyed in 2016.

On the eastern side of Baffin Island, the Koogaaluk River is partially fed by meltwater from glaciers located within the drainage basin and discharges directly into Baffin Bay. We refer to the nearshore region where the river enters Baffin Bay as the KOO estuary.

Methods

A companion paper (Alkire et al. 2017) describes the collection and analysis of water samples from ten rivers spread across Nunavut and the Northwest Territories. Here, we describe the work conducted in the estuaries directly adjoining these rivers. Note that the estuary receiving inflow from the Kangiqtuqaapik River was not studied as part of this project.

Sample Collection

Eight estuaries distributed across the CAA were visited during July and August of 2015 and 2016 (Table 1). Access to these relatively remote sites was achieved via landing a Twin Otter aircraft (Kenn Borek Air, Ltd.) on beaches and/or tundra near the mouths of the Ellice, Back and Hayes (both rivers flow into a single estuary), Kuujua, Thomsen, Cunningham, and Karasok Rivers (Fig. 1). The Coppermine River estuary was accessed directly from Kugluktuk, and the nearshore region just off the mouth of the Koogaaluk River was accessed by freighter canoe from Clyde River with the help of guides hired in association with the Illisaqsivik Society. With the exception of the Koogaaluk River region (samples collected from freighter canoes), research personnel gained access to the shallow estuaries using two inflatable boats (Achilles SPD-310) equipped with portable, outboard motors (Yamaha, 6 hp). Water samples were collected from 26 stations in 2015 and 43 stations in 2016 at nominal depths of 0.5, 1, 2, 4, 6, 8, 10, and 15 m below the surface using custom-constructed sampling rigs comprising metal plates fitting snugly over the pontoons of the boats, lengths of C-FLEX tubing (corresponding to the target depths) outfitted with plugs for pumping water, and a system of adjustable weights to keep the tubes oriented vertically in the water column. Peristaltic pump heads were attached to the ends of battery-powered drills and water was pumped upward through the tubes to the surface. After copiously flushing the tubes, water was passed through 0.45 μm , in-line filter cartridges (Pall Aquaprep 600) and collected into various bottles for chemical analyses. Salinity samples were collected into 125 mL borosilicate glass vials equipped with caps outfitted with conical polyethylene inserts. Stable oxygen isotope ($\delta^{18}\text{O}$) samples were collected into 20 mL glass vials with similarly outfitted caps. Both salinity and $\delta^{18}\text{O}$ vials were parafilm to prevent evaporation during storage and transport. Barium (Ba) samples were collected in 20 mL high-density polyethylene (HDPE) bottles that were pre-cleaned by soaking in pH 1.5 HCl overnight followed by copious rinsing with reverse osmosis deionized water (RODW). Samples for total alkalinity (TA) were collected into 125 mL I-CHEM bottles. Dissolved organic carbon (DOC) samples were collected in pre-combusted amber glass vials and acidified to pH = 2 with HCl.

CastAway CTDs (Sontek) were also deployed from each boat immediately before and after collecting water samples. Additional CTD casts were conducted throughout the estuaries, in part to help determine the position and extent of the river plumes (and corresponding salinity gradients) and identify sampling locations. Totals of 152 and 253 vertical profiles were collected during the 2015 and 2016 field seasons, respectively. The accuracies in salinity and temperature measurements are reported by the manufacturer to be 0.1 and 0.05 °C, respectively. However, after manually processing

the raw data stored onboard each instrument and comparing the computed salinities against salinities measured on discrete water samples, the accuracy of the salinity data was determined to be ± 0.2 . No alternative temperature measurements were made during the deployments. Further details describing the deployment, processing, and quality control of the data collected using these CTDs are available in the Supplementary Materials (Text S1).

All data and associated metadata are publicly available at the NSF Arctic Data Center (<https://arcticdata.io>).

Laboratory Analyses and Estimates of Uncertainty

Standards, certified reference materials, and duplicate analyses of samples were conducted in the laboratory to determine the accuracy and precision of the methods utilized to determine solute concentrations and isotopic ratios. For example, the mean precision determined from repeat analyses of the same $\delta^{18}\text{O}$ samples, separated by intervals of time ranging from hours to days, was $\pm 0.02\text{‰}$. In addition to these estimates of methodological accuracy and precision, duplicate samples were collected in the field to assess the impact of natural variations due to, for example, vertical heaving, tides, internal waves, horizontal advection, and drifting over the time scales (1–3 h) needed to collect water samples at each station. These estimates of the potential error are more conservative as they integrate both laboratory errors (quite small) and system variability encountered in the field (comparatively larger). Mean standard deviations of field duplicates (12–25 duplicates were collected for each variable during each year) yielded estimates of precision for salinity (± 0.48), $\delta^{18}\text{O}$ ($\pm 0.08\text{‰}$), TA ($\pm 14 \mu\text{eq kg}^{-1}$), Ba ($\pm 4 \text{ nmol L}^{-1}$), and DOC ($\pm 53 \mu\text{g C L}^{-1}$) during the 2015 survey. Estimates of precision for the 2016 survey were ± 0.019 (salinity), $\pm 0.07\text{‰}$ ($\delta^{18}\text{O}$), $\pm 9 \mu\text{eq kg}^{-1}$ (TA), $\pm 0.5 \text{ nmol L}^{-1}$ (Ba), and $\pm 39 \mu\text{g C L}^{-1}$ (DOC).

Oxygen isotope ratios were measured using the CO_2 equilibration method on a Finnegan Mat 251 gas source isotope ratio mass spectrometer at the Stable Isotope Laboratory, Oregon State University. Total alkalinities were determined using a Metrohm® auto-titration unit (Model 848 Titrino PLUS) according to the method of Dickson et al. (2003); accuracy was ensured through routine analyses of a certified reference material supplied by Andrew Dickson (Scripps Institute of Oceanography). Barium samples were analyzed via inductively coupled plasma mass spectrometry at the W. M. Keck Laboratory, Oregon State University. DOC concentrations were measured using a Shimadzu TOC-L analyzer at the Arizona Laboratory for Emerging Contaminants at the University of Arizona.

Salinities were measured on a Guideline Autosol Salinometer (model 8400B) at the Marine Chemistry Laboratory, University of Washington. Only a small number

of salinity samples were collected in 2015 ($n = 54$) and only two duplicate samples were collected in the field. Rather than take salinities from the CastAway CTD profiles, we instead computed salinity from chloride concentrations measured on collected water samples. The chloride concentrations were converted to salinities using the chloride/salinity ratio of 1.80655. The accuracy of the chloride-based salinities was evaluated by direct comparison against the bottle salinities. At lower salinities ($S < 26$), it was found that chloride-based salinities underestimated bottle salinities by ~ 0.1 . At higher salinities ($S \geq 26$), chloride-based salinities overestimated bottle salinities by ~ 0.6 . These biases were corrected using simple, linear regressions (intercept forced to zero) of bottle salinities versus chloride-based salinities for these lower and higher salinity ranges. At lower salinities ($S < 26$), chloride-based salinities were divided by 0.9976 (the slope of the associated regression line) and at higher salinities ($S \geq 26$), chloride-based salinities were divided by 1.0232. To assess the accuracy of this method, differences were computed between the chloride-derived salinities and those directly measured. We take the mean of the absolute values of the remaining differences (i.e., after correction) between bottle salinities and chloride-based salinities (0.48) as an estimate of the uncertainty in the salinity data reported for the 2015 survey.

Results

Salinity Sections

Vertical sections of salinity are plotted for each estuary in the panels of Fig. 3 using measurements collected via the CastAway CTDs in 2016. Many of these sections have unusual shapes/alignments; the specific set of stations in each transect was chosen to show the spatial extent of the freshwater plume/influence and the two-layered vertical structure that separated fresher surface waters from deeper, more saline waters in most of the estuaries surveyed. Vertical profiles of temperature, salinity, and corresponding T-S diagrams are available in the Supplementary Materials (Figs. S1–S3). Unsurprisingly, the estuaries receiving the largest river discharges (BHA, ELC, and COP) exhibited the largest spatial extent over which low salinities ($S < 5$) were observed. In most estuaries, the lowest salinities were vertically restricted to the topmost 1–2 m of the water column; however, the COP and TOM estuaries exhibited deeper extents of low salinity ($S < 10$) water within 4 km of the river mouths and the BHA exhibited salinities < 10 to depths of 4–6 m throughout most of the estuary.

In all of the estuaries with the exception of the KAR (salinity section not shown as the water column was homogeneous and saline), the fresher surface waters were separated

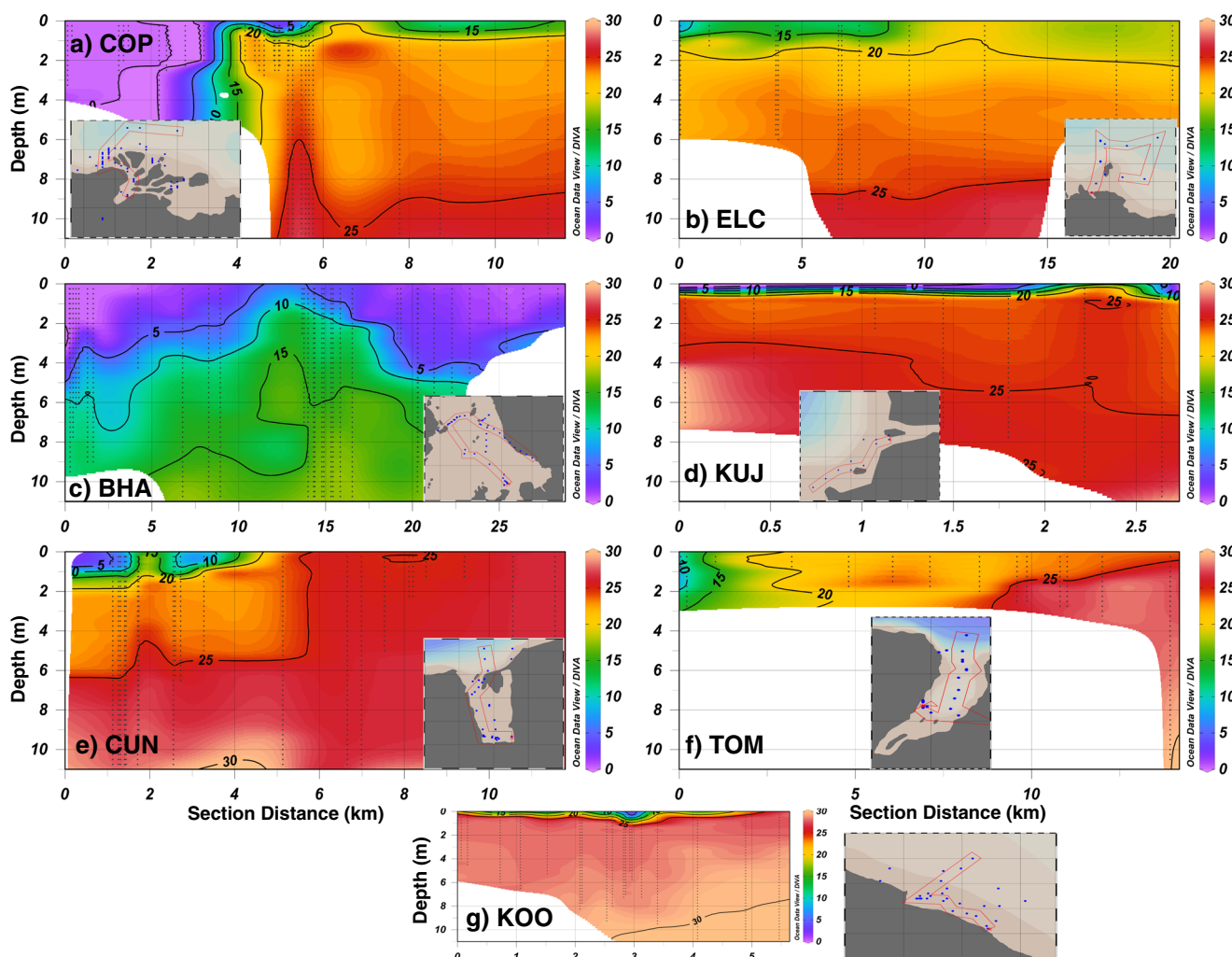


Fig. 3 Vertical sections of salinity from the **a** COP, **b** ELC, **c** BHA, **d** KUJ, **e** CUN, **f** TOM, and **g** KOO estuaries using data collected during the 2016 expedition. The KAR estuary is not shown. Colors show the salinity on a scale from 0 (cooler colors) to 30 (warmer colors); all data plotted on the same scale. Inset maps are provided in each panel to show the specific alignment of the section data. With the exception of the KOO

estuary (panel **g**), all sections start nearest to the mouth of the main river channel; in the KOO estuary, the section begins downstream (southeast) of the river mouth. The orientations of the sections were selected to provide the most complete picture of the salinity distribution in the study areas. Figures created using Ocean Data View (Schlitzer 2018)

from more saline waters at depth by strong stratification. In the ELC, CUN, TOM, and KOO estuaries, the more saline waters were also evident near the surface at stations farther offshore. We also call attention to what appear to be double cores of low-salinity water in the ELC, BHA, and CUN estuaries. These patterns result from the combination of stations included in the transects (see inset maps in Fig. 3) and indicate either plumes of low-salinity water originating from a different river (i.e., two rivers flow into the BHA) or the lateral movement of a single, low-salinity plume (i.e., ELC and CUN). For example, the ELC transect includes stations aligned in a south-to-north transect from the Ellice River mouth and then continues eastward and inshore to capture additional stations occupied downstream of the river mouth. The data show that the surface lens of low-salinity water extends ~11 km offshore of the river mouth before higher salinity waters are encountered at

the surface; however, lower salinity waters are also observed at the surface at stations to the southeast, suggesting that these lower salinity waters may extend further eastward (and closer to shore) than northward (offshore).

Scatter Plots

Plots of salinity versus $\delta^{18}\text{O}$ (Fig. 4), TA (Fig. 5), Ba (Fig. 6), and DOC (Fig. 7) show the data collected from each estuary in 2015 (blue circles) and 2016 (red squares). Also plotted in each panel of these figures are simple, linear regressions for data collected in 2015 and 2016. All regression coefficients are given in the Supplementary Materials (Tables S1–S4). The blue circles and red squares plotted on the y-axis of each panel indicate values measured directly from the rivers (values also listed in Table 1). Note that two rivers (Back and Hayes

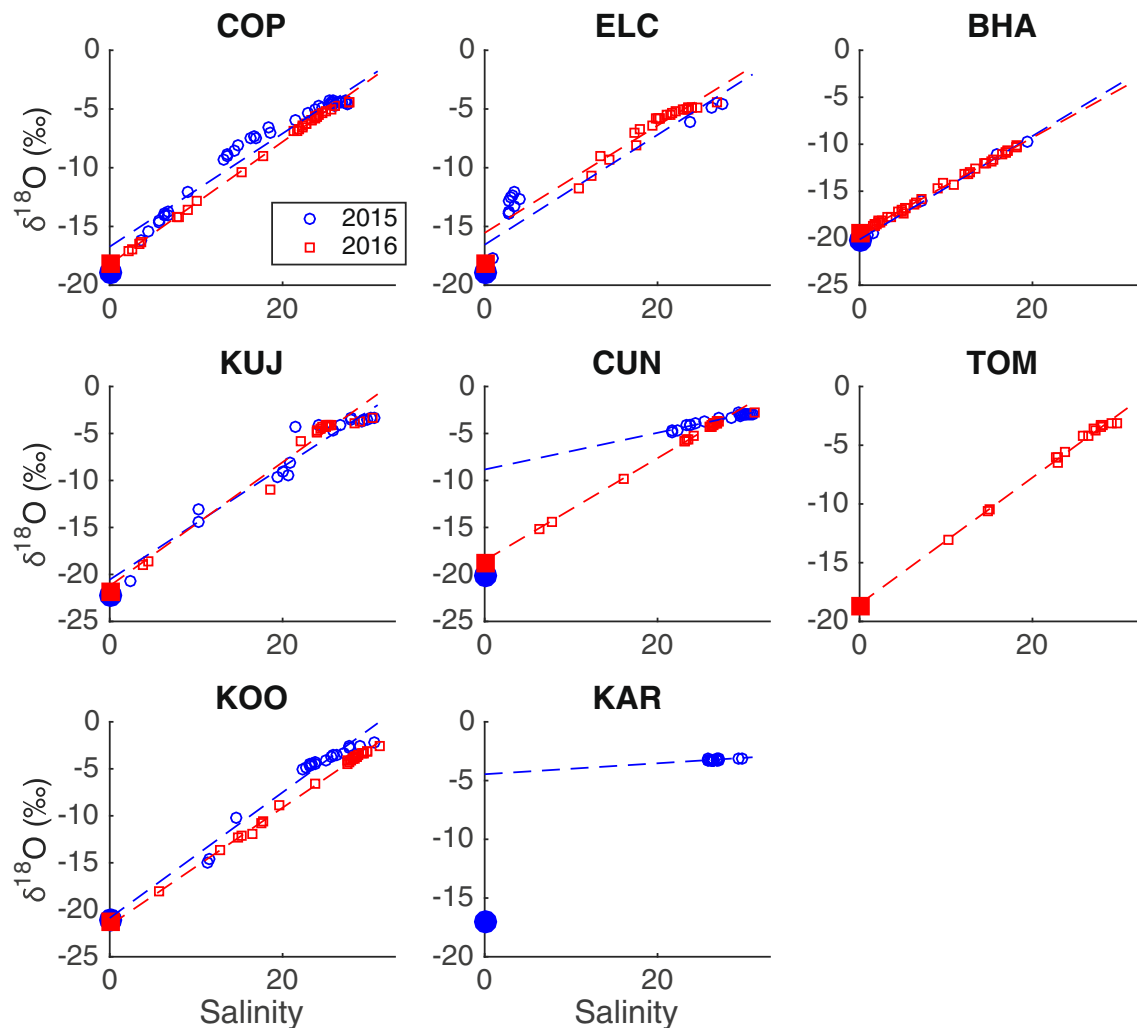


Fig. 4 Plots of stable oxygen isotope ratio ($\delta^{18}\text{O}$) versus salinity measured from water samples collected in the Coppermine (COP), Ellice (ELC), Back and Hayes (BHA), Kuujuaa (KUJ), Cunningham (CUN), Thomsen (TOM), Koogaaluk (KOO), and Karasok (KAR) estuaries during July and August of 2015 (blue circles) and 2016 (red

squares). Dashed blue and red lines indicate simple, linear regressions for the 2015 and 2016 data, respectively; regression coefficients are listed in Table S1 of the Supplementary Materials. Blue and red dots on the y-axes of the panels indicate measurements made directly on river waters entering the estuaries (values also listed in Table 2)

Rivers) enter the BHA estuary; thus, the Back River is represented by closed symbols whereas the Hayes River is represented by open symbols on corresponding panels.

The salinity and $\delta^{18}\text{O}$ data (Fig. 4) collected from most estuaries exhibited strong linear correlations between waters characterized by higher salinities ($20 < S < 31$) and more positive $\delta^{18}\text{O}$ values ($-10 < \delta^{18}\text{O} < -1\text{‰}$) and those characterized by lower, near-zero salinities and highly negative $\delta^{18}\text{O}$ ($< -15\text{‰}$). Despite these strong correlations, some estuaries (e.g., ELC and KUJ) exhibited significant scatter about the regression lines. The intercepts derived from these regressions mostly agreed with direct measurements of $\delta^{18}\text{O}$ from the rivers (Table 2 and blue dots and red squares in the panels of Fig. 4), with the exceptions of the CUN and KAR estuaries occupied in 2015. In addition, the 2015 and 2016 regressions were very similar within each estuary, with the exception of the CUN estuary (the TOM and KAR estuaries were not

sampled in both years); however, intercepts were lower (more negative) by 2‰ at COP and KUJ in 2016 (relative to 2015).

The majority of the salinity-TA data also exhibited strongly linear behavior; however, there were data points that deviated significantly from these regressions, particularly during the 2016 surveys (e.g., TOM and KUJ). The intercepts ($S = 0$) of each regression also generally agreed (within 95% confidence limits, see Table 2) with values measured directly from the rivers (Fig. 5). The sole exception was the CUN in 2015; here, the intercept greatly underestimated the river measurement. Comparing the linear regressions in each estuary between the two survey years, only the COP and CUN estuaries exhibited regression coefficients that were statistically significantly different.

The salinity-Ba regressions (Fig. 6) returned negative slopes only in the COP and TOM estuaries, indicating that these rivers acted as significant sources of barium to these

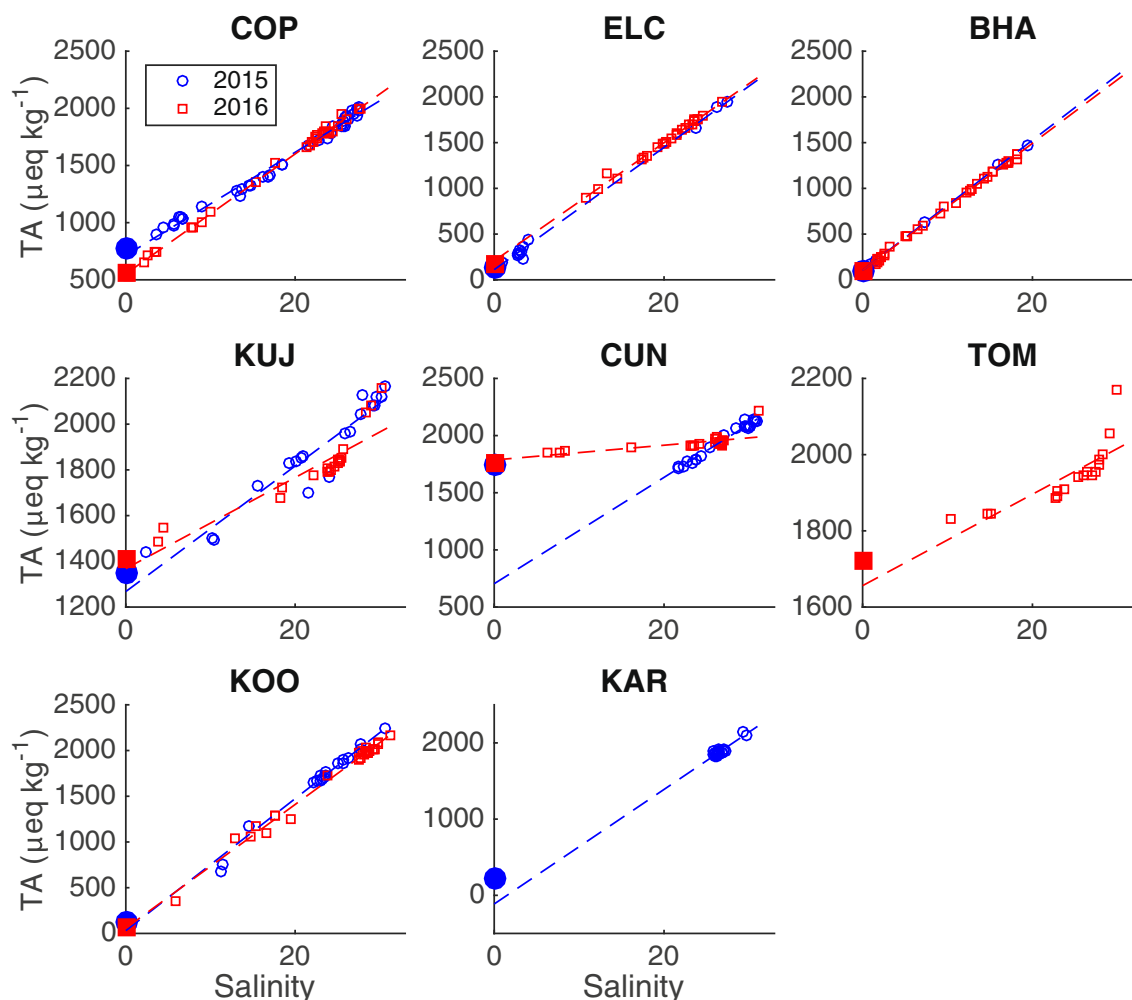


Fig. 5 Plots of total alkalinity (TA) versus salinity; regression coefficients are listed in Table S2 of the Supplementary Materials. Blue and red dots on the y-axes of the panels indicate measurements made directly on river waters entering the estuaries (values also listed in Table 2)

estuaries (relative to seawater). As was the case for TA, the majority of the derived intercepts agreed well with values measured directly in the rivers (Fig. 6 and Table 2). The 2016 COP and ELC regressions only slightly underestimated the river measurements (by < 10 nM); however, the 2015 CUN and KAR regressions greatly underestimated the river measurements (by > 40 nM) whereas the 2016 TOM regression highly overestimated the river measurement (by ~ 100 nM). The BHA regressions returned intercepts of 30–40 nM for 2015 and 2016; these values closely resembled the Ba concentrations measured in the Back River (34–37 nM) and are larger than those measured in the Hayes River (5–7 nM). The intercepts derived from the linear regressions differed only within the COP, ELC, and CUN estuaries between the 2015 and 2016 surveys.

The salinity-DOC regressions returned negative slopes in most of the estuaries studied, with the exception of the CUN and KOO (Fig. 7), indicating that these rivers generally provided a source of DOC to the estuaries (relative to seawater). The 2015 COP, ELC, and (to a small extent)

KUJ regressions underestimated the DOC measured directly in the rivers. All the other regressions returned intercepts that generally resembled the river water measurements, with the exception of the KAR (2015), which returned a negative intercept. The intercept derived from the BHA estuary data was in good agreement with, but slightly lower than, the Back River DOC measurement. Although the DOC intercepts were slightly higher in each estuary during the 2016 survey (relative to 2015), none of these differences were statistically significant at the 95% confidence level. Interestingly, the DOC concentrations measured in the rivers were slightly larger during the 2015 survey (compared to the 2016 survey).

Discussion

In general, the regressions derived from data collected in each of the estuaries sampled as part of this study returned intercepts that were in reasonable agreement with direct

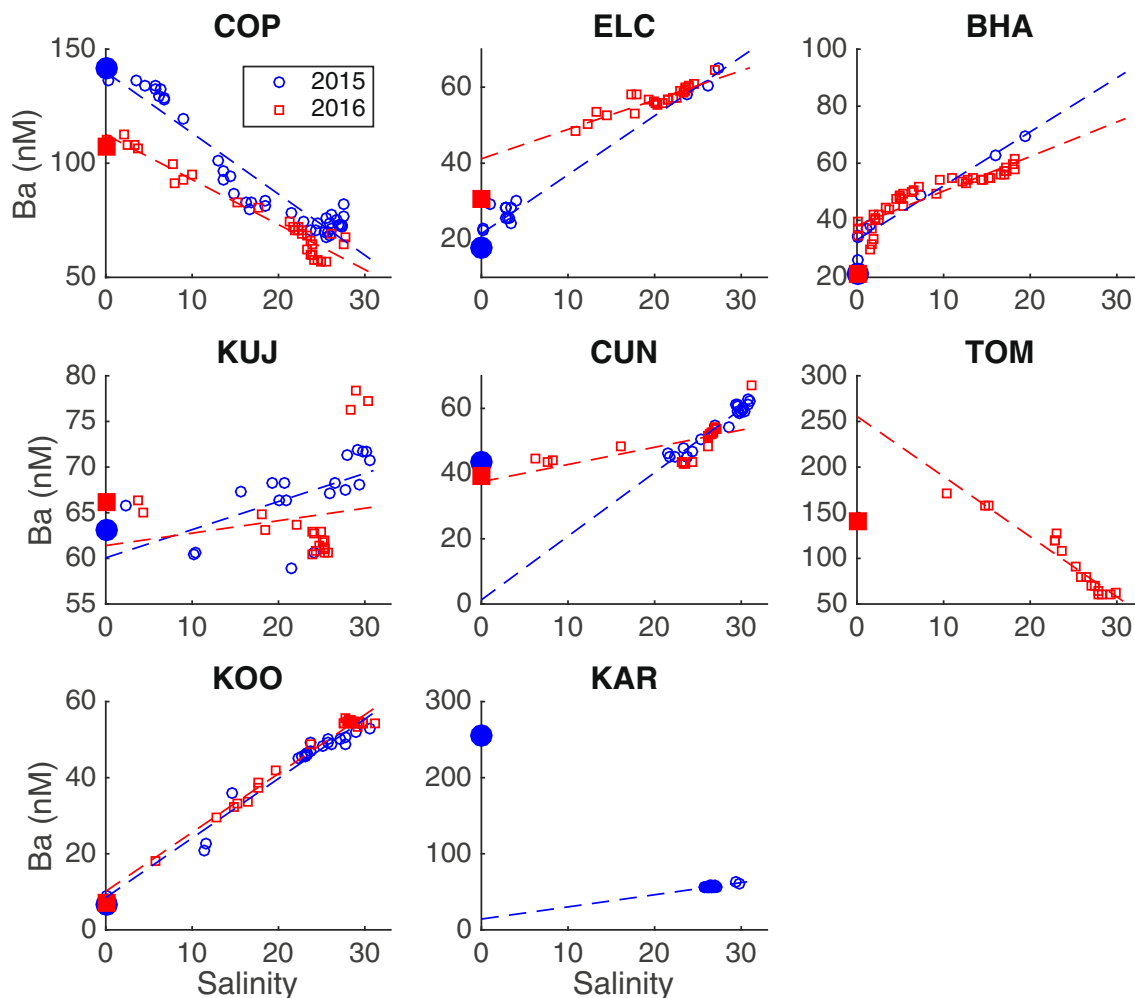


Fig. 6 Plots of barium (Ba) versus salinity; regression coefficients are listed in Table S3 of the Supplementary Materials. Blue and red dots on the y-axes of the panels indicate measurements made directly on river waters entering the estuaries (values also listed in Table 2)

measurements conducted on river water samples. This indicates that, to a large extent, the data collected from each estuary exhibited simple mixing between river water and more saline water. However, regressions that returned an intercept that differed from the value measured in the rivers and individual data points that deviated significantly from the regression denote influence from a third water type, specifically sea ice meltwater, and/or result from processes other than mixing that influence TA, Ba, and/or DOC. For example, desorption of Ba from river-borne particles during mixing with higher ionic strength waters in estuaries results in a release of Ba to the dissolved phase, increasing the dissolved barium load transported by rivers to estuaries (Guay and Falkner 1998). DOC concentrations may be increased in an estuary due to autochthonous production or biologically mediated remineralization whereas concentrations may be decreased by remineralization or photooxidation. However, less-labile fractions of DOC have been shown to resist degradation, resulting in strong linear relationships when plotted against salinity that suggest conservative mixing in some regions of

the Arctic, such as the Siberian shelves (Amon and Meon 2004; Holmes et al. 2008).

The influence of SIM by itself may impart deviations away from a simple mixing line between meteoric water/river water and saline water. Therefore, to understand the role of nonconservative processes on other measured parameters (TA, Ba, DOC), it is necessary to first quantify the relative contributions of MW and SIM within each estuary. First, salinity and $\delta^{18}\text{O}$ data are used to estimate fractional contributions of MW and SIM to each estuary. These fractions are then further analyzed to determine the vertical distributions and residence times of MW within the estuaries. Finally, the calculated fraction of SIM in each sample will be used as a basis to assess nonconservative behavior of TA, Ba, and DOC in each estuary during mixing of MW with saline water.

Water Type Analyses

Salinity and $\delta^{18}\text{O}$ have been used to separate and quantify contributions of SIM and MW throughout the Arctic (e.g.,

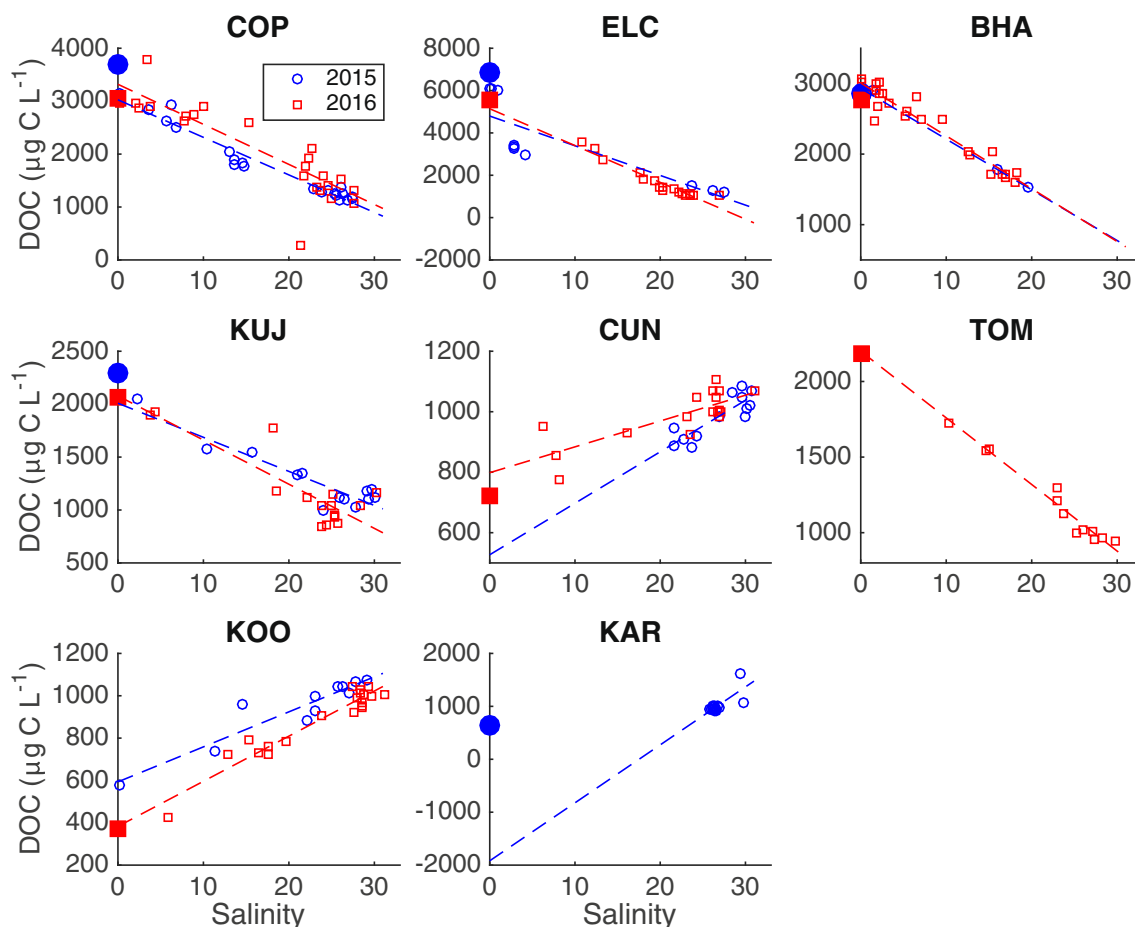


Fig. 7 Plots of dissolved organic carbon (DOC) versus salinity; regression coefficients are listed in Table S4 of the Supplementary Materials. Blue and red dots on the y-axes of the panels indicate measurements made directly on river waters entering the estuaries (values also listed in Table 2)

Yamamoto-Kawai et al. 2005, 2008; Bauch et al. 2011; Anderson et al. 2013; Alkire et al. 2015a). While SIM and

Table 1 Dates during which estuaries were surveyed in 2015 and 2016. Both calendar dates and corresponding day of year (DOY) listed for convenience. Surveyed estuaries include the Coppermine (COP), Ellice (ELC), Back and Hayes (BHA), Kuujuaa (KUJ), Cunningham (CUN), Thomsen (TOM), Koogaaluk (KOO), and Karasok (KAR)

Estuary	Sampling dates			
	2015 Calendar date	2015 DOY	2016 Calendar date	2016 DOY
COP	24–25 Jul	205–206	18–19 Aug	231–232
ELC	31 Jul	212	10 Aug	223
BHA	2 Aug	214	12, 15 Aug	225, 228
KUJ	6–7 Aug	218–219	2, 4 Aug	215, 217
CUN	12–13 Aug	224–225	22 Aug	235
TOM	–	–	8 Aug	221
KOO	21 Aug	233	27 Aug	240
KAR	10 Aug	222	–	–

MW are both characterized by low or zero salinities, they are associated with significantly different $\delta^{18}\text{O}$ values. For example, while SIM has a $\delta^{18}\text{O}$ value close to that of the seawater from which it formed (-2 to 0.3‰), river runoff and precipitation have highly negative values (-14 to -22‰) (Cooper et al. 2008). As such, these two sources of freshwater ($S=0$) can be geochemically distinguished. Given characteristic salinity and $\delta^{18}\text{O}$ values for meteoric water (S_{MW} , $\delta^{18}\text{O}_{\text{MW}}$), sea ice meltwater (S_{SIM} , $\delta^{18}\text{O}_{\text{SIM}}$), and a seawater endmember (S_{SW} , $\delta^{18}\text{O}_{\text{SW}}$), observations of salinity (S_{obs}) and $\delta^{18}\text{O}$ ($\delta^{18}\text{O}_{\text{obs}}$) in a water sample can be used to quantify the fractional contributions of these water types using a set of coupled equations:

$$S_{\text{MW}} \cdot f_{\text{MW}} + S_{\text{SIM}} \cdot f_{\text{SIM}} + S_{\text{SW}} \cdot f_{\text{SW}} = S_{\text{observed}} \quad (1)$$

$$\delta^{18}\text{O}_{\text{MW}} \cdot f_{\text{MW}} + \delta^{18}\text{O}_{\text{SIM}} \cdot f_{\text{SIM}} + \delta^{18}\text{O}_{\text{SW}} \cdot f_{\text{SW}} = \delta^{18}\text{O}_{\text{observed}} \quad (2)$$

$$f_{\text{MW}} + f_{\text{SIM}} + f_{\text{SW}} = 1 \quad (3)$$

For the MW endmember assignments, we utilized measurements conducted on water samples collected directly from the rivers within 1–2 days of the estuary surveys (Table 2). The

Table 2 Geochemical measurements conducted on water samples collected directly from rivers entering the estuaries studied during surveys conducted in 2015 and 2016. Note that the MW endmembers assigned to the BHA estuary are simple averages of measurements

collected from the Back and Hayes Rivers. Estimates of the Mean Annual Discharge (MAD), calculated by Alkire et al. (2017), are also given for each of the rivers in the last column

River	2015				2016				
	$\delta^{18}\text{O} \text{ ‰}$	TA $\mu\text{eq kg}^{-1}$	Ba nmol L^{-1}	DOC $\mu\text{g C L}^{-1}$	$\delta^{18}\text{O} \text{ ‰}$	TA $\mu\text{eq kg}^{-1}$	Ba nmol L^{-1}	DOC $\mu\text{g C L}^{-1}$	MAD $\text{m}^3 \text{ s}^{-1}$
COP	−18.99	768	141.7	3691	−18.23	562	107.3	3040	224
ELC	−18.99	140	17.9	6857	−18.21	180	30.7	5550	77.6
BAK	−20.16	111	37.3	3630	−19.41	127	34.3	3116	494
HAY	−20.30	67	4.6	2097	−19.69	54	6.8	2407	98.7
KUJ	−22.22	1347	63.1	2290	−21.84	1412	66.2	2064	70.5
CUN	−20.10	1742	43.3	—	−18.83	1756	39.4	722	10.4
TOM	—	—	—	3823	−18.71	1720	140.5	2183	50.5
KOO	−21.07	116	6.8	—	−21.22	68	7.2	370	8.59
KAR	−16.99	222	254.5	634	—	—	—	—	1.03

salinity and $\delta^{18}\text{O}$ values assigned to SW (Table 3) were typically chosen from the most saline sample collected in each estuary during each year of occupation; however, exceptions were made to this general rule if an examination of the data suggested that the most saline water sampled did not accurately represent the SW that was more thoroughly mixed throughout the estuary. For example, higher salinity, near-bottom waters might have been recently advected into the study region via tidal action or denser waters might have collected into a depression in the bottom topography. In such cases, examination of the scatter diagrams helped to identify these potential outliers and assign alternate endmember values. In one case (CUN), the same endmembers were utilized during both years as the deeper water sampled in 2016 likely reflected brine-influenced waters in a bottom depression.

Prior studies of Arctic estuaries have similarly assigned saline water endmembers based upon observations and/or expectations of the most saline water mass entering an estuary. Working in the Beaufort Sea region, Macdonald et al. (1995) described the polar mixed layer saline water mass as the “salinity of water at the depth to which winter mixing by brine-driven convection and winter stirring has occurred.” The specific properties of this saline water mass may change from year to year, depending upon the conditions in the estuary during the winter preceding the summer surveys; however, we note that the salinity and $\delta^{18}\text{O}$ of the saline waters were quite similar in each estuary during both sampling years, indicating consistent conditions. By selecting the most saline water sample collected, we are assuming that waters lying either below or offshore/outside the influence of MW and SIM represent the relatively homogeneous and saline conditions that were likely present in each estuary prior to the onset of peak river discharge and sea ice melt in May/June.

Fewer data are available to assign salinity and $\delta^{18}\text{O}$ characteristic/endmember values to SIM. We have therefore characterized sea ice melt water using a universal salinity of 6 to represent first-year, landfast ice (Macdonald et al. 1995; Alkire et al. 2015b) and a $\delta^{18}\text{O}$ value estimated via applying a fractionation factor of +2‰ to the $\delta^{18}\text{O}$ value assigned to the SW endmember. Two samples of sea ice were collected from the TOM estuary in August 2016 to help verify these choices. The salinities (0.2 and 1.8) were relatively low, as might be expected for first-year ice that has likely lost most of its brine content by the late summer period when the samples were collected. However, the $\delta^{18}\text{O}$ measurements (−1.29 and −1.05‰) agreed well with the endmember assignment: −3.08‰ (the SW endmember in the TOM estuary) + 2‰ (fractionation factor) = −1.08‰. Fractionation factors during sea ice formation vary depending on ice growth rates, thickness, and age but typically range between 1.6 and 2.6‰ in field observations (Macdonald et al. 1995; Melling and Moore 1995; Eicken 1998; Alkire et al. 2015b). One may assume that the fractionation factor should be applied to surface water observations, since the sea ice is formed (and melted) at the surface. However, this treatment assumes that the properties of the water at the time of observation match the properties that characterized the water column at the time of ice formation. Since ice formation likely began during late autumn/early winter, during a period of minimal river discharge, the salinity and $\delta^{18}\text{O}$ were most likely quite different from those observed during summer months. Therefore, rather than apply the fractionation factor to surface $\delta^{18}\text{O}$ measurements in the estuaries that would implicitly incorporate some MW contribution, the fractionation factors were instead applied to the SW definitions (Macdonald et al. 1995).

We recognize this approach may underestimate the MW contribution to sea ice (i.e., river ice); however, we argue that

Table 3 Endmember assignments for saline water (SW) in each estuary. Values shown in parentheses were estimated via linear interpolation; estimates were made when specific measurements were missing (i.e., no sample collected) or measurements were deemed anomalous/poor quality. For the CUN, the endmember assignments defined in 2015 were used again in 2016 (see text for details)

Estuary	Salinity	$\delta^{18}\text{O}$ (‰)	TA $\mu\text{eq kg}^{-1}$	Ba nmol L^{-1}	DOC $\mu\text{g C L}^{-1}$
2015					
COP	27.512	−4.56	1987	81.8	1151
ELC	27.464	−4.64	1956	65	1201
BHA	19.489	−9.71	1463	69.6	1536
KUJ	30.561	−3.33	2164	70.8	(1025)
CUN	30.967	−2.92	2119	62.4	(1054)
TOM	—	—	—	—	—
KOO	30.667	−2.28	2247	52.7	(1100)
KAR	27.146	−3.19	1900	57.2	(1054)
2016					
COP	27.665	−4.42	1997	67.7	1070
ELC	26.926	−4.4	1941	64.4	1083
BHA	18.192	−10.27	1379	61.5	(1645)
KUJ	30.302	−3.43	2155	77.2	1165
CUN	(30.967)	(−2.92)	(2119)	(62.4)	(1054)
TOM	29.85	−3.08	(2055)	61.6	945
KOO	31.275	−2.52	2161	54.1	1007
KAR	—	—	—	—	—

the contribution of river ice in these estuaries during the summer periods over which the surveys were conducted was likely small. Most of these rivers are quite small and winter flow is very low or zero; thus, any river ice introduced to the system would result from the small amount of river water left in the estuary prior to freeze-up or ice entering the estuary from the river during the spring floods. As our surveys occurred well after the spring floods, we expect that most of the landfast ice and river ice was melted and/or pushed offshore prior to sample collection. Nevertheless, we have explored the possibility of larger influences from river ice meltwater (see Supplementary Materials Text S4) and the results indicated river ice melt may have been present in a small number of samples collected from the COP, KUJ, CUN, and TOM estuaries.

In order to obtain an unbiased estimate of the uncertainties in the water type analysis, we adopted an approach previously utilized by Alkire et al. (2015a). This method assigns a realistic range of endmember values (rather than a specific value) and runs the analyses through a number of iterations ($n = 1000$) wherein the endmembers used to compute each set of water type fractions is randomly selected from the assigned range. This random selection is based on a uniform distribution; thus, each value in the assigned endmember range is weighted equally. In contrast, a normal distribution puts a higher weight on the preferred/central endmember assignment. The ranges in endmember values were estimated by computing the standard deviations of the $\delta^{18}\text{O}_{\text{MW}}$, $\delta^{18}\text{O}_{\text{SW}}$, and S_{SW} values from each field year and multiplying them by two. For example, the $\delta^{18}\text{O}_{\text{MW}}$ measured in the Coppermine River (−18.99‰ in 2015 and −18.23‰ in

2016) yields a standard deviation of 0.53‰; multiplying this value by two yields an estimate of uncertainty for $\delta^{18}\text{O}_{\text{MW}}$ equal to ± 1.07 ‰. This uncertainty was then used to define a possible range in $\delta^{18}\text{O}_{\text{MW}}$ for each year. For 2015, the $\delta^{18}\text{O}_{\text{MW}}$ ranged between −20.06 and −17.92‰; for 2016, it ranged between −19.30 and −17.16‰. As very few measurements of the salinity and $\delta^{18}\text{O}$ of sea ice were available, we instead chose to assign a salinity range from 2 to 10 and varied the fractionation factor that is applied to the $\delta^{18}\text{O}_{\text{SW}}$ endmember value between 1.5 and 2.5. Overall, this approach produced 1000 different solutions (MW, SIM, and SW fractions) for each sample (i.e., each salinity, $\delta^{18}\text{O}$ pair). The averages of these solutions are taken as the optimal values for the MW, SIM, and SW fractions. The corresponding standard deviations are used to assign uncertainties to the calculated fractions.

The mean standard deviations of MW, SIM, and SW estimated via this analysis were 0.01, 0.02, and 0.02, respectively. The maximum standard deviations were 0.05 for MW, 0.12 for SIM, and 0.11 for SW. It is notable to point out that MW and SIM fractions encountered offshore in the deep basins of the Arctic Ocean typically range between 0 and 0.20 (for MW) and −0.12 and +0.12 (for SIM) (e.g., Yamamoto-Kawai et al. 2005). The MW fractions within the surveyed estuaries are much higher, as should be expected due to the proximity to the river mouths. The largest standard deviations in the calculated MW fractions typically occurred at higher values (> 0.5) that are not often observed farther offshore. In contrast, the majority of the higher uncertainties in SIM were associated with the range of fractions that are regularly

observed in offshore regions. This finding should be of particular interest to Arctic freshwater studies as large uncertainties in the calculated SIM fractions will complicate (and perhaps even inhibit) attempts to discriminate among certain freshwater sources, such as North American versus Siberian river water influences, using geochemical tracers (e.g., Yamamoto-Kawai et al. 2005; Alkire et al. 2010).

Finally, we note that water type fractions computed using endmember values that were individually assigned to each estuary at the time of sampling represent seasonal, rather than net annual, values; in other words, the computed fractions do not have a “memory” of prior MW, SIM, or SW influence. Instead, fractions calculated represent the influence of the defined water types during (or close to) the period of sampling. This is convenient in that MW contributions can be compared to river discharge that occurred close in time to the survey periods. Such a comparison provides a first-order estimate of the residence time of river runoff in each estuary.

Vertical Distributions of MW and SIM Fractions

MW fractions in the CUN and KAR estuaries were very low in 2015, and the vertical profiles exhibited little change with depth (Fig. 8). All other estuaries exhibited a significant MW

influence that was highest near the surface and decreased with depth to values ≤ 0.02 (essentially indistinguishable from zero given the uncertainty in the water type analyses). In general, estuaries receiving freshwater inflow from comparatively large rivers (see Table 2) exhibited a deeper influence of MW. For example, stations occupied within the ELC had significant MW fractions down to 4 m depth, and the COP and BHA had even deeper (6–8 m) influences. In contrast, MW fractions were restricted to the top ~2 m within estuaries associated with lower river discharges (KUJ, TOM, KOO, and CUN). These vertical profiles also indicated larger MW fractions in most of these estuaries in 2015 compared to 2016. Some of this variability was a consequence of sampling in slightly different locations and at slightly different times (Table 1) in the estuaries in 2015 compared to 2016; however, samples collected from repeated stations do suggest more MW was present in most of these estuaries in 2015.

Vertical profiles of SIM also generally indicated larger contributions in 2015 compared to 2016 (Fig. 9). SIM fractions were also generally lower than MW fractions in most estuaries, except for the CUN and KAR estuaries in 2015. SIM profiles generally decreased with increasing depth, but the COP, ELC, KUJ, and KOO estuaries all exhibited a mid-depth maximum in SIM. This feature is coincident with an

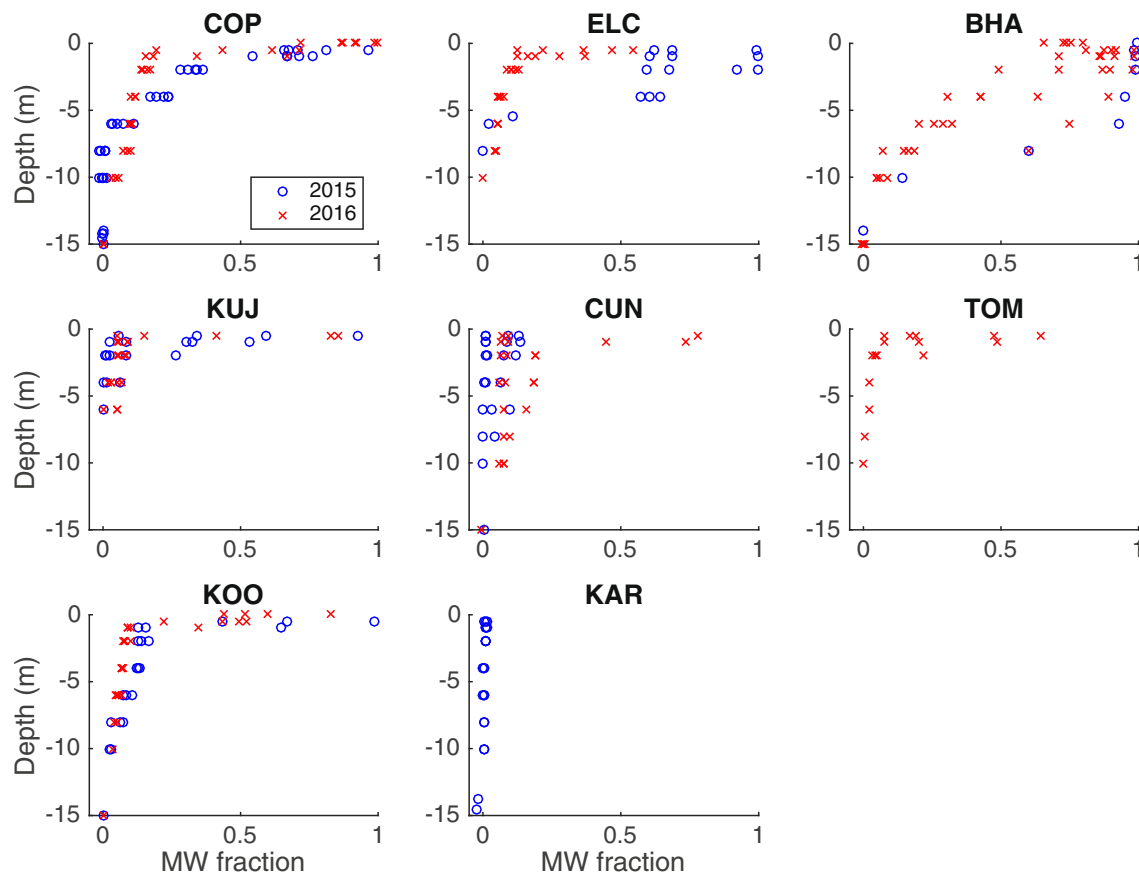


Fig. 8 Vertical profiles of meteoric water (MW) fractions from the estuaries surveyed in 2015 (blue circles) and 2016 (red x's)

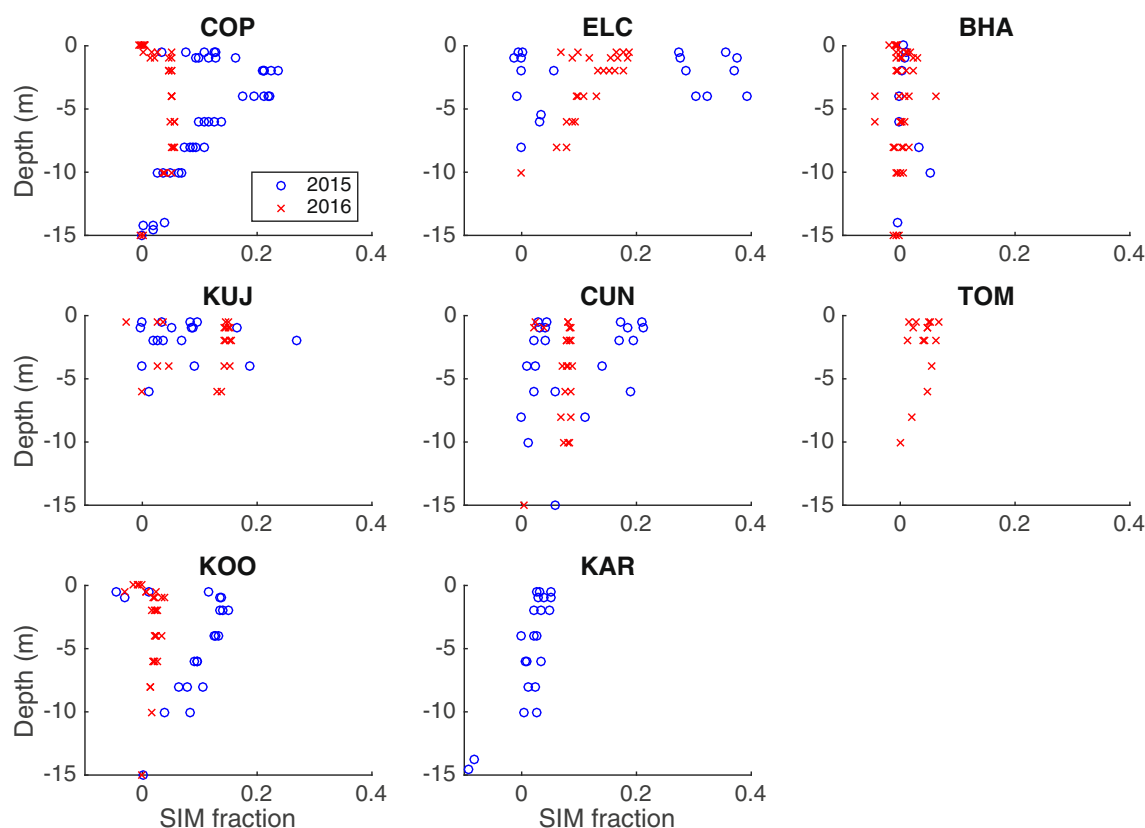


Fig. 9 Vertical profiles of sea ice meltwater (SIM) fractions from the estuaries surveyed in 2015 (blue circles) and 2016 (red x's)

intermediate water mass identified in the T-S diagrams (see Fig. S3 in the Supplementary Materials). This intermediate water mass might have been formed by mixing between SW and SIM (perhaps early in the season or farther offshore) and then subducted beneath fresher outflow from the rivers. Significant contributions of SIM were also found at greater depths compared to MW fractions. Penetration of SIM was particularly deep (~10 m) in the COP, CUN, KOO, and KAR estuaries. The apparent penetration of SIM could be a consequence of enhanced mixing by winds or tides of less stratified waters in the CUN, KOO, and KAR estuaries where weak (or no) river inflow was apparent. In contrast, the higher SIM fractions at depth in the more highly stratified COP estuary could indicate mixing prior to or during the spring freshet, essentially allowing relatively fresh SIM to vertically mix throughout most of the water column prior to the strong stratification that comes with a high rate of river input (e.g., Alkire and Trefry 2006).

Plots of MW versus SIM fractions (Fig. 10) provide additional insights into the mechanisms responsible for the observed distributions of both these freshwater sources. For example, the COP estuary has two semi-linear relationships in 2015 that meet at a single apex associated with the maximum SIM fraction in the estuary in 2015. The positive-slope branch, indicating an increase

in both MW and SIM fractions, represents measurements collected at depths below 2–4 m whereas the negative-slope branch, indicative of increasing MW but decreasing SIM fractions, represents measurements collected from depths ≤ 2 m.

We hypothesize that the positive-slope branch results from the break up and melting of landfast ice that includes contributions from both sea ice and river ice in the early part of the summer. The freshening that occurs during this stage yields a weak stratification of the estuary that is strengthened by increasing river input during the spring freshet (period of maximum discharge). The second stage produces the negative-slope branch as river runoff becomes the predominant source of freshwater in the estuary during late summer and the sea ice cover is pushed offshore by prevailing winds, currents, and/or the river plume itself. As the summer progresses, there is less sea ice available for melt but river runoff continues to enter the estuarine system, resulting in the muted patterns observed in the estuaries during the 2016 survey.

Inventories and Residence Times

The total freshwater fraction (FW) is equal to the sum of MW and SIM fractions; however, total freshwater may also

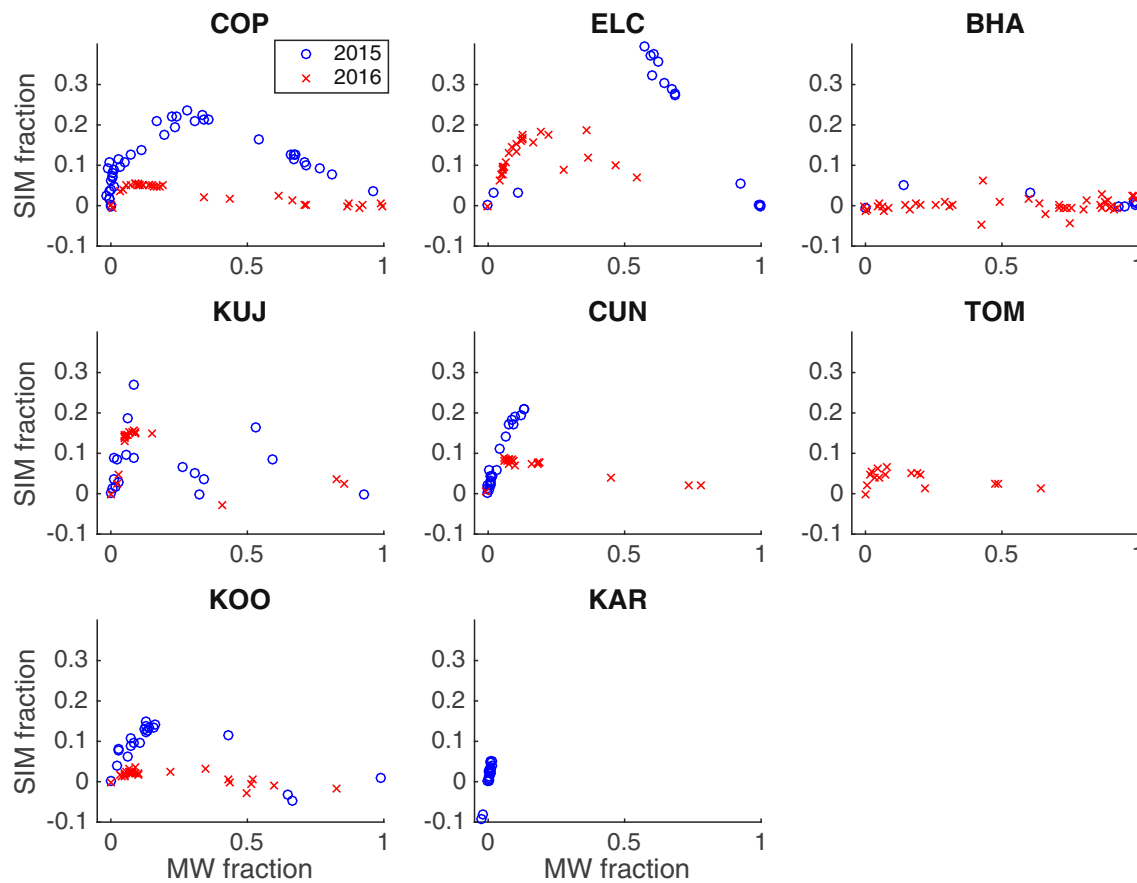


Fig. 10 Fractions of sea ice meltwater (SIM) plotted against meteoric water (MW) from the estuaries surveyed in 2015 (blue circles) and 2016 (red x's)

be calculated from salinity profiles (such as those measured by the CastAway CTDs) after assigning an appropriate reference salinity (S_{ref}), chosen simply as the SW salinity in each estuary during 2015 and 2016:

$$FW = \frac{S_{ref} - S_{observed}}{S_{ref}} \quad (4)$$

Fractional contributions of FW, MW, and SIM were interpolated onto a 0.25-m grid, assuming the water column was homogeneous between the surface (0 m) and 0.25 m, and integrated with depth to obtain contributions in terms of inventories (in meters). Since the collection of water samples was limited to 4–5 stations per estuary, the mean MW and SIM inventories from these stations were compared to estimate the proportion of total FW from MW in each estuary: $MW/(MW + SIM)$. These proportions were then multiplied by the mean total FW inventories calculated using the more extensive CTD profiles to approximate the mean inventory of MW in each estuary. The mean volume of MW was then computed by multiplying the mean inventory by a rough estimate of the area of each survey region using the Ruler/Polygon tool in

GoogleEarth Pro. These mean MW volumes were then divided by the river discharge (see Table 2) to obtain first-order estimates of the residence time of river water in each estuary. Additional details describing the calculations are available in Text S2 of the Supplementary Materials and the results are summarized in Table 4.

Most of the residence times calculated for the estuaries occupied in 2015 and 2016 ranged between <1 and <6 days; however, residence times were considerably longer in the Koogaaluk (KOO) and Cunningham (CUN) estuaries (23–45 days). These longer residence times may have resulted from the very low river discharges that supply MW to these estuaries. Alternatively, the longer residence time in the KOO estuary might have resulted from additional MW sources (such as iceberg melt) and complex circulation mechanisms. We acknowledge that the majority of these residence times are likely inaccurate due to the (necessary) use of the mean annual discharge rates rather than (unavailable) daily discharges during the actual survey periods. The residence times calculated for the COP, ELC, and BHA estuaries should be more accurate as they incorporated river discharge rates measured during the survey periods. Although these residence times

Table 4 Mean meteoric water (MW), sea ice meltwater (SIM), and total freshwater (FW) inventories for the estuaries surveyed. Italicized values of river discharge rates represent the mean daily discharges during the days the surveys were conducted. No discharge data available for the Back River in 2016, so we assumed discharge in 2015 was equal to that in 2016. All other rivers are ungauged; therefore, mean annual discharge

rates computed by Alkire et al. (2017) were used in place of daily discharge rates during the time of the surveys. The Karasok estuary (KAR) was excluded from this analysis as no significant MW influence was encountered during the surveys. Insufficient data were collected from the BHA and TOM estuaries in 2015 to allow for the calculation of residence times

Estuary	Area (km ²)	MW (m)	SIM (m)	MW/(MW + SIM)	FW (m)	Discharge (m ³ s ⁻¹)	Residence time (days)
2015							
COP	32	2.1	1.5	0.6	2.6	332	1.7
ELC	70	3.4	0.9	0.8	2.4	475	3.2
BHA	119	—	—	—	—	1180	—
KUJ	8	0.6	0.3	0.7	0.6	70.5	0.5
CUN	35	0.2	0.5	0.3	0.7	10.4	7.8
TOM	38	—	—	—	—	50.5	—
KOO	24	1.5	1	0.6	1.9	8.6	36.8
2016							
COP	32	1.4	0.4	0.8	1.5	316.5	1.4
ELC	70	0.8	0.7	0.5	1.3	98.5	5.7
BHA	119	4.8	0	1.0	3.7	1180	4.3
KUJ	8	0.5	0.5	0.5	1.3	70.5	0.9
CUN	35	1.1	0.7	0.6	1.9	10.4	45.2
TOM	38	0.5	0.2	0.7	0.5	50.5	3.1
KOO	24	0.8	0.2	0.8	0.9	8.6	23.3

are highly uncertain, they suggest that river waters generally move through each of these estuaries over the course of a few days.

Assessing Nonconservative Behaviors

Total Alkalinity

It is expected that TA should not be subject to significant, nonconservative behavior in these estuaries. In addition, the total alkalinities of MW and SW have been directly measured and assigned from our observations. We will therefore assume we can explain the majority of the observed variability in TA as mixing between the MW (river) and SW endmembers in each estuary. We will then examine the influence of SIM fractions on the remaining TA, or TA anomaly:

$$TA_{anomaly} = TA_{measured} - (TA_{MW} * f_{MW}) - (TA_{SW} * f_{SW}) \quad (5)$$

We have already shown that, in most of the estuaries studied, the primary source of variability in the data is explained by mixing between MW and SW; the contribution from SIM is comparatively small. Equation 5 removes this main axis of variation, and assuming the remaining TA

has been supplied by SIM, a significant correlation between the $TA_{anomaly}$ and f_{SIM} suggests that SIM is responsible for the majority of the “remaining” TA and the slope of the linear regression (assuming an intercept equal to zero) provides an estimate for the TA_{SIM} that best fits the data.

An examination of the plots of $TA_{anomaly}$ vs. f_{SIM} (Fig. 11) indicates that the majority of the TA anomalies were positively correlated with (and therefore explained by) the SIM fractions. The dashed line plotted in each of these panels indicates an average $TA_{SIM} = 500 \mu\text{eq kg}^{-1}$. Most of the TA anomalies plot on or near this line, suggesting that $500 \mu\text{eq kg}^{-1}$ is a reasonable (if not completely accurate) assignment for TA_{SIM} in each estuary. Scatter around this line indicates instances where TA_{SIM} was likely higher or lower than this median value; this is not surprising given the high spatial and temporal variability associated with sea ice chemistry (e.g., Miller et al. 2011; Alkire et al. 2015b). However, some of the data exhibit consistent deviation from this average value that might reflect a nonconservative process, presence of an additional (and unaccounted for) water mass, and/or error in the assignment of MW and/or SW endmember values. Given the uncertainties in the TA measurements as well as those associated with the calculation of the MW, SIM, and SW fractions, only anomalies exceeding $\pm 50 \mu\text{mol kg}^{-1}$ are

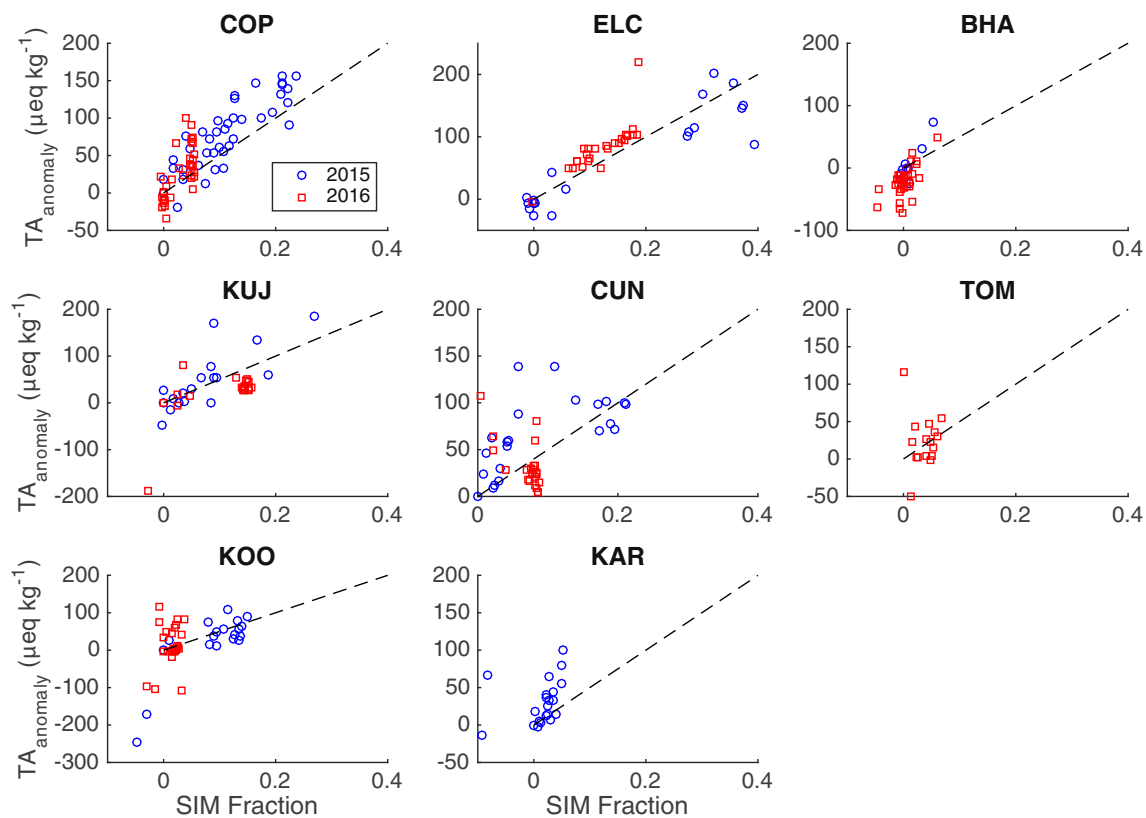


Fig. 11 Fractions of sea ice meltwater (SIM) vs. total alkalinity (TA) anomalies, calculated as the difference between TA measurements and predicted values based on mixing between river and seawater endmembers from the estuaries surveyed in 2015 (blue circles) and 2016 (red squares)

considered to be significant. Smaller anomalies are indistinguishable from the propagated uncertainty in the calculations.

A positive anomaly indicates that the simple mixing model between MW and SW produces a TA that is less than the observed value. In such a case, a positive contribution of TA from SIM would provide the “missing” TA. In contrast, a negative anomaly indicates that the mixing model has exceeded the observed TA value. Negative anomalies likely result from errors in the assignment of endmember values and/or the presence of additional water masses that have not been considered. The negative anomalies observed in the 2016 KOO and KUJ estuaries were associated with near-surface waters exhibiting significant contributions from MW. We speculate that these data might reflect an influence from an additional, low-TA water type, such as glacial meltwater or direct precipitation. Larger TA contributions associated with SIM could indicate the dissolution of authigenic precipitates (such as ikaite) or the presence of river ice melt. Although we were not able to confirm either of these possibilities with the available data, a separate water type analysis incorporating salinity, $\delta^{18}\text{O}$, and TA (details provided in the Supplementary Materials Text

S4) indicated that a small amount of river ice melt may have been present in the COP, KUJ, CUN, and TOM estuaries.

Barium

Barium anomalies generally correlated positively with SIM fractions, indicating that SIM explains the majority of the additional variability in the Ba distributions in these estuaries (Fig. 12). The dashed lines in the panels of Fig. 12 indicate that Ba concentrations of 30 nM reasonably characterized SIM in most of the estuaries surveyed. However, larger positive anomalies (anomalies exceeding $\pm 6 \text{ nmol L}^{-1}$ are considered to be significant) were observed in the COP, TOM, and BHA estuaries that reflect additional sources of variability. For the COP, the highest Ba anomalies coincided with salinities ranging between 4.5 and 13; this salinity range has been found in other studies to be optimal for the release of barium adsorbed onto river-borne particles (Guay and Falkner 1998). A similar process likely also occurred in the TOM estuary in 2016 as the highest Ba anomalies were associated with a similar salinity range.

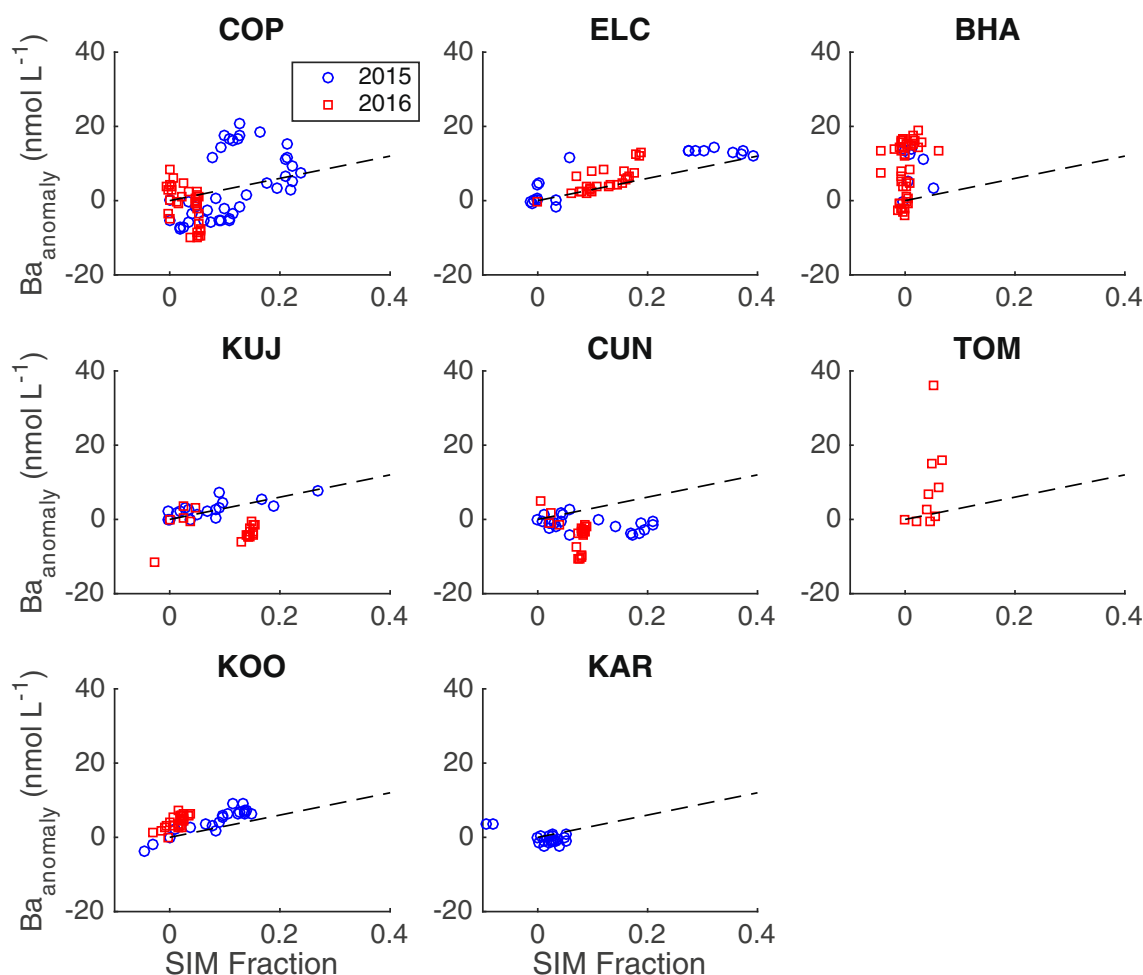


Fig. 12 Fractions of sea ice meltwater (SIM) vs. barium (Ba) anomalies from the estuaries surveyed in 2015 (blue circles) and 2016 (red squares)

Anomalies observed in the BHA likely resulted from the influence of two different rivers (Back and Hayes Rivers) with different characteristic Ba concentrations (though similar $\delta^{18}\text{O}$ and TA, see Table 2). The Ba concentrations assigned to MW for the calculation of the anomalies were simple averages of the measurements from the Back and Hayes Rivers. The largest Ba anomalies coincided with stations sampled on the eastern side of the estuary where influence from the Hayes River was most likely concentrated. These results suggest that Ba might be used to separate the contributions of the Back and Hayes Rivers in this estuary.

Dissolved Organic Carbon

Positive correlations between dissolved organic carbon (DOC) anomalies and SIM fractions were observed in the COP estuary in 2015 and the BHA, ELC, and KOO estuaries during 2016; all other estuaries exhibited weak or no correlations (Fig. 13). Large negative anomalies (anomalies exceeding $\pm 100 \mu\text{g C L}^{-1}$ are considered to be significant) were observed in the COP, ELC, BHA, and KUJ estuaries

during both survey years, indicating the mixing model exceeded the observed DOC concentrations. These results imply removal of DOC from the estuaries or gross errors in the assignment of endmembers. Since these anomalies were generally associated with lower salinity waters nearest the surface, we speculate that photobleaching and/or biologically mediated remineralization may be responsible. As we do not have the data necessary to assess the quality/labability of the DOC, we cannot further address this issue and recommend it as an important topic of investigation for future studies.

Larger positive anomalies ($> 500 \mu\text{g C L}^{-1}$) were observed only in the COP estuary during the 2016 survey. Since these anomalies were not correlated with SIM, alternate sources are required to account for the DOC, such as the remineralization of particulate organic matter and/or the release of DOC from river-borne suspended particulates during estuarine mixing. It is clear from these observations that DOC should not be relied upon as a tracer of MW or SIM in these estuaries as some degree of nonconservative behavior has influenced the distribution of DOC. We recommend further studies address the organic carbon budget in these estuaries, particularly measurements of

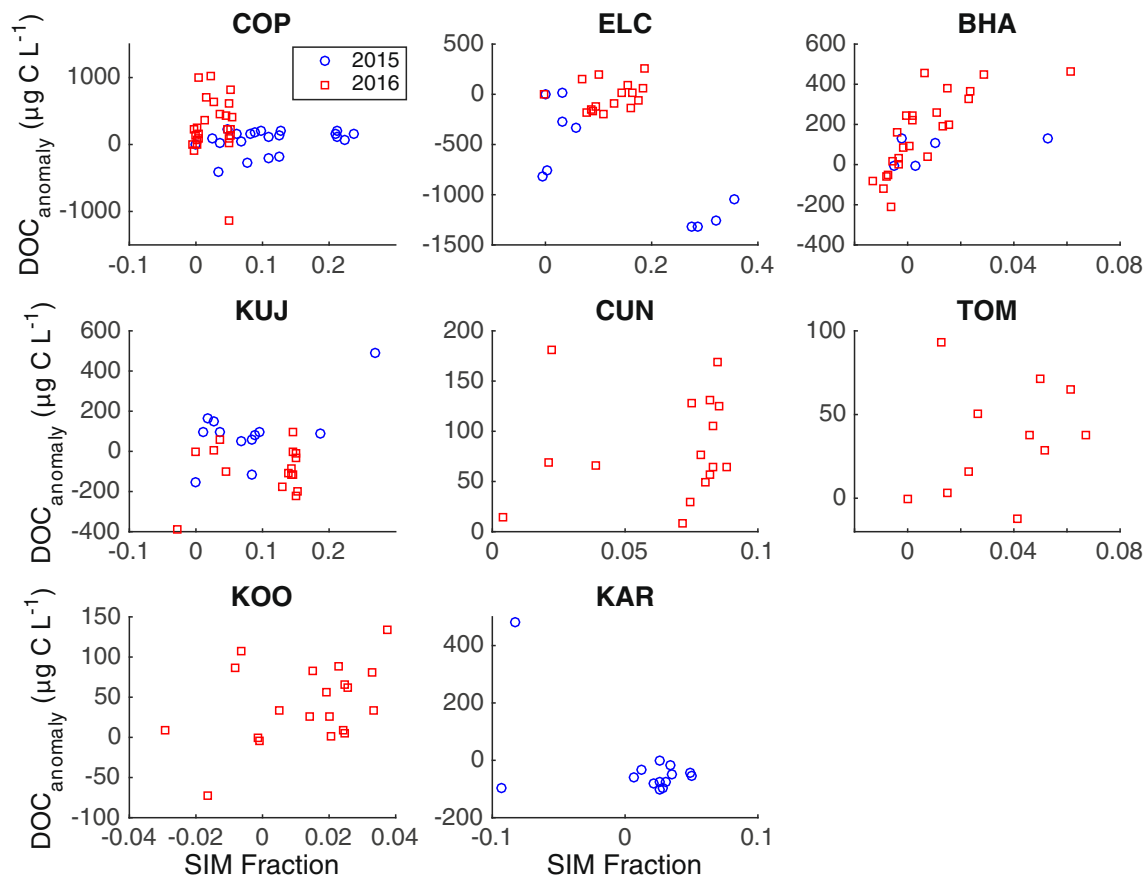


Fig. 13 Fractions of sea ice meltwater (SIM) vs. dissolved organic carbon (DOC) anomalies from the estuaries surveyed in 2015 (blue circles) and 2016 (red squares)

colored dissolved organic matter, to determine what processes are influencing DOC concentrations other than mixing.

Conclusions

In most of the estuaries studied, scatter plots of MW and SIM fractions indicated two depth-dependent, semi-linear relationships that we have interpreted to represent different mixing regimes. The concurrent melting of sea ice and release of river waters during the spring flood period resulted in a positive relationship between MW and SIM for depths > 2 m. Subsequently, a negative relationship between MW and SIM becomes prevalent at shallower depths (≤ 2 m) as runoff continues to enter the estuaries, providing additional stratification, and sea ice is mostly exported offshore and away from the estuary. Estimated inventories of MW equaled or exceeded the inventories of SIM in each estuary, indicating that most of the freshwater originated from rivers regardless of the magnitude of discharge or the geometry of the estuaries.

Residence times of river runoff were predominately on the order of 1–8 days; longer residence times were restricted to estuaries (CUN and KOO) receiving the lowest ($< 10 \text{ m}^3 \text{ s}^{-1}$) mean annual river discharges. Most residence times (with the

exception of COP, ELC, and BHA) were likely underestimated due to the use of mean annual discharges, rather than instantaneous discharges measured during the surveys. Additional uncertainties were introduced via the need to extrapolate limited geochemical data to CTD-based estimates of total freshwater content. Despite these uncertainties, the results indicate that river water typically moves through these estuaries and progresses offshore in less than 1 week.

Derived contributions of MW, SIM, and SW were combined with measurements of TA, Ba, and DOC to offer an improved method for geochemically characterizing SIM in mixing models as well as to identify and quantify the impact of nonconservative processes that may complicate the use of some tracers to separate the contributions from different freshwater sources in the Arctic and subarctic seas. Rather than arbitrarily select a single value to represent, for example, the TA of SIM, “anomalies” were defined based on the mixing between MW and SW. The slope of a linear regression between these anomalies and SIM fractions returned an average value that generally characterized the geochemistry of SIM in these regions: $500 \mu\text{eq kg}^{-1}$ (TA) and 30 nmol L^{-1} (Ba). Large and/or consistent deviations away from a linear relationship between these anomalies and SIM fractions indicated nonconservative behavior, an additional water mass, and/or errors in

the assignment of endmember values in the water type analysis. For example, Ba anomalies that did not strongly correlate with SIM fractions in the COP and TOM estuaries provided evidence suggesting a small (≤ 20 nM), additional source from the desorption of barium on river-borne particles during estuarine mixing. Anomalies in the DOC concentrations were observed in most of the estuaries studied and indicated significant remineralization; we therefore suggest DOC not be utilized as a tracer of freshwater sources in CAA estuaries.

Our results have broader implications for oceanographic studies. For example, relatively high uncertainties in the water type analyses were associated with large SIM contributions but only intermediate MW contributions. The magnitudes of these fractions are well within the range of fractions that are typically computed/encountered in studies conducted in deeper waters of the Arctic Ocean and the CAA. If such uncertainties apply to nearshore regions where river runoff first enters the marine system, they also apply to regions farther offshore where MW influences are somewhat lower and may originate from numerous sources. Such uncertainties should be considered when employing MW and SIM fractions for various analytical methods, such as the correction of linear regressions for influences from sea ice melt or formation (e.g., Yamamoto-Kawai et al. 2005; Alkire et al. 2010).

Acknowledgements The Hunters and Trappers Organizations in Kugluktuk, Cambridge Bay, Gjoa Haven, and Ulukhaktok as well as the Illisaqsiq Society (Clyde River) were contacted for guidance, consultation, and support both before and during field work. Representatives from these organizations aided in the hiring of local residents to act as wildlife monitors and provided logistical support to facilitate access to river and estuary sampling sites. This work would not have been possible without their kind and valuable support and the authors thank them very much for their invaluable efforts. We would like to especially thank Barbara Adjun, Dianne Mala, Betty Haogak, Jakob Gearheard, Nelson Perry, Renee Wissink, Tessum Weber, and Barbara Masaki for their efforts in helping to plan and support field work. Field assistance provided by John Kelly and Gabriella Kitch during the summer sampling campaigns was highly appreciated. We also thank Thomas Quinn, Pascal Schuback, and Matt Irinaga for their outstanding logistical support and safety planning prior to field operations. Finally, we thank Wally Dobchuk, James Haffey, Steve King, Douglas Westersund, Tyler Best, and Stephen Martyniuk from Kenn Borek Air, Ltd. for safely and securely transporting the research team to the field sites.

All data presented in this paper are publicly available on the project website (www.canadianriversproject.org), as well as the NSF Arctic Data Center (<https://arcticdata.io>).

This research was supported by U.S. National Science Foundation Office of Polar Programs grants to Alkire (PLR-1303766) and Jacobson (PLR-1304675). Any opinions, findings, and conclusions or recommendations expressed in this material are those of the author(s) and do not necessarily reflect the views of the National Science Foundation.

Open Access This article is distributed under the terms of the Creative Commons Attribution 4.0 International License (<http://creativecommons.org/licenses/by/4.0/>), which permits unrestricted use, distribution, and reproduction in any medium, provided you give appropriate credit to the original author(s) and the source, provide a link to the Creative Commons license, and indicate if changes were made.

References

- Aagaard, K., and E.C. Carmack. 1989. The role of sea ice and other fresh water in the Arctic circulation. *Journal of Geophysical Research* 94 (C10): 14485–14498.
- Alkire, M.B., and J.H. Trefry. 2006. Transport of spring floodwater from rivers under ice to the Alaskan Beaufort Sea. *Journal of Geophysical Research* 111 (C12008). <https://doi.org/10.1029/2005JC003446>.
- Alkire, M.B., K.K. Falkner, J. Morison, R.W. Collier, C.K. Guay, R.A. Desiderio, I.G. Rigor, and M. McPhee. 2010. Sensor-based profiles of the NO parameter in the central Arctic and southern Canada Basin: new insights regarding the cold halocline. *Deep-Sea Research Part I* 57 (11): 1432–1443.
- Alkire, M.B., J. Morison, and R. Andersen. 2015a. Variability in the meteoric water, sea-ice melt, and Pacific water contributions to the central Arctic Ocean, 2000–2014. *Journal of Geophysical Research* 120: 1573–1598. <https://doi.org/10.1002/2014JC010023>.
- Alkire, M.B., F. Nilsen, E. Falck, J. Søreide, and T. Gabrielsen. 2015b. Tracing sources of freshwater contributions to first-year sea ice in Svalbard fjords. *Continental Shelf Research* 101: 85–97.
- Alkire, M.B., A. Jacobson, G.O. Lehn, R.W. Macdonald, and M.W. Rossi. 2017. On the geochemical heterogeneity of rivers draining into the straits and channels of the Canadian Arctic Archipelago. *Journal of Geophysical Research – Biogeosciences* 122: 2527–2547. <https://doi.org/10.1002/2016JG003723>.
- AMAP. 2013. *AMAP Assessment 2013: Arctic Ocean Acidification*. Oslo, Norway: Arctic Monitoring and Assessment Programme (AMAP) viii + 99 pp.
- Amon, R., and B. Meon. 2004. The biogeochemistry of dissolved organic matter and nutrients in two large Arctic estuaries and potential implications for our understanding of the Arctic Ocean system. *Marine Chemistry* 92: 311–330.
- Amon, R.M.W., G. Budeus, and B. Meon. 2003. Dissolved organic carbon distribution and origin in the Nordic Seas: exchanges with the Arctic Ocean and the North Atlantic. *Journal of Geophysical Research* 108 (C7). <https://doi.org/10.1029/2002JC001594>.
- Andersson, L.G., P.S. Andersson, G. Björk, E.P. Jones, S. Jutterström, and I. Wählström. 2013. Source and formation of the upper halocline of the Arctic Ocean. *Journal of Geophysical Research* 118 (1–12): 410–421. <https://doi.org/10.1029/2012JC008291>.
- Azetsu-Scott, K., A. Clarke, K. Falkner, J. Hamilton, E.P. Jones, C. Lee, B. Petrie, S. Prinsenberg, M. Starr, and P. Yeats. 2010. Calcium carbonate saturation states in the waters of the Canadian Arctic Archipelago and the Labrador Sea. *Journal of Geophysical Research* 115 (C11). <https://doi.org/10.1029/2009JC005917>.
- Azetsu-Scott, K., B. Petri, P. Yeats, and C. Lee. 2012. Composition and fluxes of freshwater through Davis Strait using multiple chemical tracers. *Journal of Geophysical Research* 117 (C12011). <https://doi.org/10.1029/2012JC008172>.
- Bauch, D., M.R. van der Loeff, N. Andersen, S. Torres-Valdes, K. Bakker, and E.P. Abrahamsen. 2011. Origin of freshwater and polynya water in the Arctic Ocean halocline in summer 2007. *Progress in Oceanography* 91 (4): 482–495. <https://doi.org/10.1016/j.pocean.2011.07.017>.
- Carmack, E.C., P. Winsor, and W. Williams. 2015. The contiguous panarctic Riverine Coastal Domain: a unifying concept. *Progress in Oceanography* 139: 13–23. <https://doi.org/10.1016/j.pocean.2015.07.014>.
- Chierici, M., and A. Fransson. 2009. Calcium carbonate saturation in the surface water of the Arctic Ocean: undersaturation in freshwater influenced shelves. *Biogeosciences* 6: 2421–2432.
- Comiso, J.C., C.L. Parkinson, R. Gersten, and L. Stock. 2008. Accelerated decline in the Arctic sea ice cover. *Geophysical Research Letters* 35 (L01703). <https://doi.org/10.1029/2007GL031972>.

- Cooper, L.W., J.W. McClelland, R.M. Holmes, P.A. Raymond, J.J. Gibson, C.K. Guay, and B.J. Peterson. 2008. Flow-weighted values of runoff tracers ($\delta^{18}\text{O}$, DOC, Ba, alkalinity) from the six largest Arctic rivers. *Geophysical Research Letters* 35 (18). <https://doi.org/10.1029/2008GL035007>.
- Déry, S.J., M.A. Hernández-Henríquez, J.E. Burford, and E.F. Wood. 2009. Observational evidence of an intensifying hydrological cycle in northern Canada. *Geophysical Research Letters* 36 (L13402). <https://doi.org/10.1029/2009GL038852>.
- Dickson, A., J. Afghan, and G. Anderson. 2003. Reference materials for oceanic CO_2 analysis: a method for the certification of total alkalinity. *Marine Chemistry* 80 (2): 185–197.
- Dodd, P.A., B. Rabé, E. Hansen, E. Falck, A. Mackensen, E. Rohling, C. Stedmon, and S. Kristiansen. 2012. The freshwater composition of the Fram Strait outflow derived from a decade of tracer measurements. *Journal of Geophysical Research* 117 (C11). <https://doi.org/10.1029/2012JC008011>.
- Eicken, H. 1998. Deriving modes and rates of ice growth in the Weddell Sea from microstructural salinity and stable-isotope data. In *Antarctic sea ice: Physical processes, interactions and variability (Antarctic Research Series)*, ed. M.O. Jeffries, vol. 74, 89–122. Washington, D.C.: AGU.
- Falck, E., G. Kattner, and G. Budeus. 2005. Disappearance of Pacific water in the northwestern Fram Strait. *Geophysical Research Letters* 32 (14). <https://doi.org/10.1029/2005GL023400>.
- Fichot, C.G., K. Kaiser, S.B. Hooker, R.M.W. Amon, M. Babin, S. Belanger, S.A. Walker, and R. Benner. 2013. Pan-Arctic distributions of continental runoff in the Arctic Ocean. *Scientific Reports* 3 (1053). <https://doi.org/10.1038/rep01053>.
- Gardner, A.S., G. Moholdt, B. Wouters, G.J. Wolken, D.O. Burgess, M.J. Sharp, J.G. Cogley, C. Braun, and C. Labine. 2011. Sharply increased mass loss from glaciers and ice caps in the Canadian Arctic Archipelago. *Nature* 473: 357–360.
- Granskog, M.A., C.A. Stedmon, P.A. Dodd, R.M.W. Amon, A. Pavlov, L. de Steur, and E. Hansen. 2012. Characteristics of colored dissolved organic matter (CDOM) in the Arctic outflow in Fram Strait: assessing the changes and fate of terrigenous CDOM in the Arctic Ocean. *Journal of Geophysical Research* 117 (C12021). <https://doi.org/10.1029/2012JC008075>.
- Guay, C.K., and K.K. Falkner. 1997. Barium as a tracer of Arctic halocline and river waters. *Deep-Sea Research Part II* 44 (8): 1543–1569.
- Guay, C.K., and K.K. Falkner. 1998. A survey of dissolved barium in the estuaries of major Arctic rivers and adjacent seas. *Continental Shelf Research* 18 (8): 859–882.
- Guay, C.K., G.P. Klinkhammer, K.K. Falkner, R. Benner, P.G. Coble, T.E. Whitledge, B. Black, F.J. Bussell, and T.A. Wagner. 1999. High-resolution measurements of dissolved organic carbon in the Arctic Ocean by *in situ* fiber-optic spectrometry. *Geophysical Research Letters* 26 (8): 1007–1010.
- Guay, C.K., F.A. McLaughlin, and M. Yamamoto-Kawai. 2009. Differentiating fluvial components of upper Canada Basin waters on the basis of measurements of dissolved barium combined with other physical and chemical tracers. *Journal of Geophysical Research* 114. <https://doi.org/10.1029/2008JC005099>.
- Guéguen, C., L. Guo, M. Yamamoto-Kawai, and N. Tanaka. 2007. Colored dissolved organic matter dynamics across the shelf-basin interface in the western Arctic Ocean. *Journal of Geophysical Research* 112 (C05038). <https://doi.org/10.1029/2006JC003584>.
- Haine, T.W.N., B. Curry, R. Gerdes, E. Hansen, M. Karcher, C. Lee, B. Rudels, G. Spreen, L. de Steur, K.D. Stewart, and R. Woodgate. 2015. Arctic freshwater export: status, mechanisms, and prospects. *Global & Planetary Change* 125: 13–356.
- Holmes, R.M., J.W. McClelland, P.A. Raymond, B.B. Frazer, B.J. Peterson, and M. Stieglitz. 2008. Lability of DOC transported by Alaskan rivers to the Arctic Ocean. *Geophysical Research Letters* 35 (L03402). <https://doi.org/10.1029/2007GL032837>.
- Jahn, A., L.B. Tremblay, R. Newton, M.M. Holland, L.A. Mysak, and I.A. Dmitrenko. 2010. A tracer study of the Arctic Ocean's liquid freshwater export variability. *Journal of Geophysical Research* 115 (C07015). <https://doi.org/10.1029/2009JC005873>.
- Jones, E.P., and A.R. Coote. 1980. Nutrient distribution in the Canadian Archipelago: indicators of summer water mass and flow characteristics. *Canadian Journal of Fishery and Aquatic Sciences* 37 (4): 589–599.
- Jungclauss, J.H., H. Haak, M. Esch, E. Roeckner, and J. Marotzke. 2006. Will Greenland melting halt the thermohaline circulation. *Geophysical Research Letters* 33 (17). <https://doi.org/10.1029/2006GL026815>.
- Kliem, N., and D.A. Greenberg. 2003. Diagnostic simulations of the summer circulation in the Canadian arctic archipelago. *Atmosphere-Ocean* 41 (4): 273–289.
- Macdonald, R.W., D.W. Paton, and E.C. Carmack. 1995. The freshwater budget and under-ice spreading of Mackenzie River water in the Canadian Beaufort Sea based on salinity and $^{18}\text{O}/^{16}\text{O}$ measurements in water and ice. *Journal of Geophysical Research* 100 (C1): 895–919.
- McClelland, J.W., R.M. Holmes, K.H. Dunton, and R.W. Macdonald. 2012. The Arctic Ocean estuary. *Estuaries and Coasts* 35 (2): 353–368.
- Melling, H. 2000. Exchanges of fresh-water through the shallow straits of the North American Arctic. In *The freshwater budget of the Arctic Ocean*, ed. E.L. Lewis, E.P. Jones, P. Lemke, T.D. Prowse, and P. Wadhams, 479–502. Dordrecht: Kluwer Academic Publishers.
- Melling, H., and R.M. Moore. 1995. Modification of halocline source waters during freezing on the Beaufort Sea shelf: evidence from oxygen isotopes and dissolved nutrients. *Continental Shelf Research* 15 (1): 89–113.
- Melling, H., T.A. Agnew, K.K. Falkner, D.A. Greenberg, C.M. Lee, A. Munchow, B. Petrie, S.J. Prinsenberg, R.M. Samelson, and R.A. Woodgate. 2008. Fresh-water fluxes via Pacific and Arctic outflows across the Canadian polar shelf. In *Arctic-subarctic ocean fluxes: defining the role of the northern seas in climate*, ed. R.R. Dickson, J. Meincke, and P. Rhines, 193–247. Berlin: Springer.
- Miller, L.A., T.N. Papakyriakou, R.E. Collins, J.W. Deming, J.K. Ehn, R.W. Macdonald, A. Mucci, O. Owns, M. Raudsepp, and N. Sutherland. 2011. Carbon dynamics in sea ice: a winter flux time series. *Journal of Geophysical Research* 116 (C02028). <https://doi.org/10.1029/2009JC006058>.
- Pavlov, A.K., M.A. Granskog, C.A. Stedmon, B.V. Ivanov, S.R. Hudson, and S. Falk-Petersen. 2015. Contrasting optical properties of surface waters across the Fram Strait and its potential biological implications. *J. Mar. Sys.* 143: 62–72.
- Peterson, B.J., J. McClelland, R. Curry, R.M. Holmes, J.E. Walsh, and K. Aagaard. 2006. Trajectory shifts in the Arctic and subarctic freshwater cycle. *Science* 313: 1061–1066.
- Prinsenberg, S.J., and J. Hamilton. 2005. Monitoring the volume, fresh-water and heat fluxes passing through Lancaster sound in the Canadian arctic archipelago. *Atmosphere-Ocean* 43: 1–22.
- Proshutinsky, A., R.H. Bourke, and F.A. McLaughlin. 2002. The role of the Beaufort Gyre in Arctic climate variability: seasonal to decadal climate scales. *Geophysical Research Letters* 29 (23): 15-1–15-4. <https://doi.org/10.1029/2002GL015847>.
- Rignot, E., M. Koppes, and I. Velicogna. 2010. Rapid submarine melting of the calving faces of West Greenland glaciers. *Nature Geoscience* 3 (3): 187–191. <https://doi.org/10.1038/ngeo765>.
- Schlitzer, R. (2018). *Ocean data view*, <https://odv.awi.de>.
- Serreze, M.C., A.P. Barrett, A.G. Slater, R.A. Woodgate, K. Aagaard, R.B. Lammers, M. Steele, R. Moritz, M. Meredith, and C.M. Lee. 2006. The large-scale freshwater cycle of the Arctic. *Journal of*

- Geophysical Research* 111 (C11010). <https://doi.org/10.1029/2005JC003424>.
- Stroeve, J.C., M.C. Serreze, M.M. Holland, J.E. Kay, J. Maslanik, and A.P. Barrett. 2011. The Arctic's rapidly shrinking sea ice cover: a research synthesis. *Climatic Change* 110 (3–4): 1005–1027. <https://doi.org/10.1007/s10584-011-0101-1>.
- Taylor, J.R., K.K. Falkner, U. Schauer, and M. Meredith. 2003. Quantitative considerations of dissolved barium as a tracer in the Arctic Ocean. *Journal of Geophysical Research* 108. <https://doi.org/10.1029/2002JC001635>.
- Torres-Valdes, S., T. Tsubouchi, S. Bacon, A.C. Naveira-Garabato, R. Sanders, F.A. McLaughlin, B. Petrie, G. Kattner, K. Azetsu-Scott, and T.E. Whitledge. 2013. Export of nutrients from the Arctic Ocean. *Journal of Geophysical Research* 118 (4): 1625–1644. <https://doi.org/10.1002/jgrc.20063>.
- Washam, P., A. Münchow, and K. Nicholls. 2018. A decade of ocean changes impacting the ice shelf of Petermann Gletscher. *Journal of Physical Oceanography*, in press 48 (10): 2477–2493.
- Woodgate, R.A., T.J. Weingartner, and R. Lindsay. 2012. Observed increases in Bering Strait oceanic fluxes from the Pacific to the Arctic from 2001 to 2011 and their impacts on the Arctic Ocean water column. *Geophysical Research Letters* 39 (L24603). <https://doi.org/10.1029/2012GL054092>.
- Yamamoto-Kawai, M., N. Tanaka, and S. Pivovarov. 2005. Freshwater and brine behaviors in the Arctic Ocean deduced from historical data of $\delta^{18}\text{O}$ and alkalinity (1929–2002 A.D.). *Journal of Geophysical Research* 110 (C10). <https://doi.org/10.1029/2004JC002793>.
- Yamamoto-Kawai, M., E. Carmack, and F. McLaughlin. 2006. Nitrogen balance and Arctic throughflow. *Nature* 443: 43.
- Yamamoto-Kawai, M., F.A. McLaughlin, E.C. Carmack, S. Nishino, and K. Shimada. 2008. Freshwater budgets of the Canada Basin, Arctic Ocean, from salinity, $\delta^{18}\text{O}$, and nutrients. *Journal of Geophysical Research* 113 (C1). <https://doi.org/10.1029/2006JC003858>.
- Yamamoto-Kawai, M., E.C. Carmack, F.A. McLaughlin, and K.K. Falkner. 2010. Oxygen isotope ratio, barium and salinity in waters around the north American coast from the Pacific to the Atlantic: implications for freshwater sources to the Arctic throughflow. *Journal of Marine Research* 68 (1): 97–117.